# APPENDIX A

**PATENT**

IN THE UNITED STATES PATENT AND TRADEMARK OFFICE

| | |
|---|---|
| In re Application of:<br>David J. Yang *et al.* | Group Art Unit: 1618 |
| Serial No.: 10/672,763 | Examiner: Jones, Dameron Levest |
| Filed: September 26, 2003 | Atty. Dkt. No.: UTSC:664USC1 |
| For: Ethylenedicysteine (EC)-Drug Conjugates, Compositions and Methods for Tissue Specific Disease Imaging | |

**DECLARATION OF DAVID J. YANG, CHUN-WEI LIU, DONG-FANG YU, AND E. EDMOND KIM UNDER 37 C.F.R. § 1.131**

We, David J. Yang, Chun-Wei Liu, Dong-fang Yu, and E. Edmond Kim, hereby declare as follows:

1. We are the joint inventors of the subject matter claimed in the above-referenced patent application.

2. We are submitting this declaration to set forth facts demonstrating that the invention as reflected in the claims of the above referenced patent application was reduced to practice prior to June 1, 1999.

3. Attached as Exhibit 1 is an abstract and summary of our studies pertaining to the invention as reflected in the claims of the above-referenced patent application. Each of the documents set forth in Exhibit 1 was prepared prior to June 1, 1999.

4. Exhibit 1 demonstrates that the invention was reduced to practice.

5. In particular, reduction to practice of the claimed methods of imaging a site within a subject is shown by the fact that we prepared compositions of particular radionuclide-labeled bis-aminoethanethiol (BAT) dicarboxyxlic acid-targeting ligand conjugates and detected radioactive signals by emission tomography in subjects following administration of the compositions to the subjects. Information regarding the preparation and imaging using the BAT dicarboxylic acid-targeting ligand conjugates which we studied is summarized as follows:

- $^{99m}$Tc-ethylenedicysteine (EC)-folate – Information regarding the synthesis of EC-folate, radiolabeling of EC-folate with $^{99m}$Tc, and scintigraphic imaging and autoradiography studies using $^{99m}$Tc-EC-folate in Fischer rats can be found in Example 1 (pages 4-6 and 11) and FIGS. 4-6 of Exhibit 1.
- $^{99m}$Tc-EC-metronidazole (MN) – Information regarding the synthesis of EC-MN, radiolabeling of EC-MN with $^{99m}$Tc, and scintigraphic imaging and autoradiography studies using $^{99m}$Tc-EC-MN in Fischer rats can be found in Example 2 (pages 6-8 and 12), Table 4, and FIGS. 11-15 of Exhibit 1.
- $^{99m}$Tc-EC-nitroimidazole (NIM) – Information regarding the synthesis of EC-NIM, radiolabeling of EC-NIM with $^{99m}$Tc, and scintigraphic imaging and autoradiography studies using $^{99m}$Tc-EC-NIM in Fischer rats can be found in Example 2 (pages 6-8 and 12), Table 4, and FIGS. 11-15 of Exhibit 1.
- $^{99m}$Tc-EC-pentaglutamate (GAP) – Information regarding the synthesis of EC-GAP, radiolabeling of EC-GAP with $^{99m}$Tc, and scintigraphic imaging and autoradiography studies using $^{99m}$Tc-EC-GAP in Fischer rats can be found in Example 3 (pages 9 and 12)

and FIG. 17 of Exhibit 1.

- $^{99m}$Tc-EC-Annexin V (ANNEX) – Information regarding the synthesis of EC-ANNEX, radiolabeling of EC-ANNEX with $^{99m}$Tc, and scintigraphic imaging and autoradiography studies using $^{99m}$Tc-EC-ANNEX in Fischer rats can be found in Example 4 (page 9, 13) and FIGS. 18-20 of Exhibit 1.
- $^{99m}$Tc-EC-colchicine (COL) – Information regarding the synthesis of EC-COL, radiolabeling of EC-COL with $^{99m}$Tc, and scintigraphic imaging and autoradiography studies using $^{99m}$Tc-EC-COL in Fischer rats can be found in Example 5 (pages 10-11 and 13) and FIGS. 22-27 of Exhibit 1.

6. In conclusion, we reduced to practice the invention as reflected in the claims of the above-referenced patent application prior to June 1, 1999.

7. We hereby declare that all statements made by our own knowledge are true and all statements made on information and belief are believed to be true and further that statements were made with the knowledge that willful false statements and the like so made are punishable by fine or imprisonment under § 100 of Title 18 of the United States Code, and that such willful false statements may jeopardize the validity of this application or any patent issued thereon.

Date: 7/18/2006 David J. Yang

David J. Yang

Date: 7/18/2006 William C. Liu

Chun-Wei Liu

Date: 7-18-06 Dong-Fang Yu

Dong-Fang Yu

Date: 7/18/2006

E. Edmond Kim, MD.

E. Edmond Kim

# EXHIBIT 1

# Ethylenedicysteine (EC)-Drug Conjugates for Tumor Targeted Imaging

## ABSTRACT

Radionuclide imaging modalities (positron emission tomography, PET; single photon emission computed tomography, SPECT) are diagnostic cross-sectional imaging techniques that map the location and concentration of radionuclide-labeled radiotracers. Although CT and MRI provide considerable anatomic information about the location and the extent of tumors, these imaging modalities cannot adequately differentiate invasive lesions from edema, radiation necrosis, grading or gliosis. PET and SPECT can be used to localize and characterize tumors by measuring metabolic activity.

Due to favorable physical characteristics as well as extremely low price ($0.21/mCi), technetium ($^{99m}$Tc, t1/2=6 hours) has been preferred to label radiopharmaceuticals for SPECT. $^{99m}$Tc can be obtained from a $^{99}$Mo/$^{99m}$Tc generator. Among $^{99m}$Tc chelators, $^{99m}$Tc-L,L-ethylenedicysteine ($^{99m}$Tc-EC) is the most recent and successful example. We have then developed a series of new ligands conjugated with EC.

Strategies for the application of these ligands can be categorized in three ways: (1) prediction of therapeutic response; we developed folate receptors targeting ligands: $^{99m}$Tc-EC-folate, $^{99m}$Tc-EC-methotrexate ($^{99m}$Tc-EC-MTX), $^{99m}$Tc-EC-tomudex ($^{99m}$Tc-EC-TDX), (2) monitoring tumor response to treatment; we developed imaging ligands for tumor apoptotic cells, angiogenesis and tumor hypoxia. These ligands are $^{99m}$Tc-EC-annexin V (EC-ANNEX), $^{99m}$Tc-EC-colchicine (EC-COL), $^{99m}$Tc-EC-2-nitroimidazole and $^{99m}$Tc-EC-metronidazole, (3) differential diagnosis and differentiation of malignancies; we developed $^{99m}$Tc-EC-glutamate pentapeptide.

These ligands are designed for functional imaging by SPECT so that a better tumor treatment response is expected. The ligands are stored in kit forms.

**TITLE: Ethylenedicysteine (EC)-Drug Conjugates for Tumor Targeted Imaging**

## 8.0. INTRODUCTION

### a. Invention Description

**What it does and how it can be used**

Improvement of scintigraphic tumor imaging is extensively determined by development of more tumor specific radiopharmaceuticals. Due to greater tumor specificity, radiolabeled ligands as well as radiolabeled antibodies have opened a new era in scintigraphic detection of tumors and undergone extensive preclinical development and evaluation[1]. Radionuclide imaging modalities (positron emission tomography, PET; single photon emission computed tomography, SPECT) are diagnostic cross-sectional imaging techniques that map the location and concentration of radionuclide-labeled radiotracers. Although CT and MRI provide considerable anatomic information about the location and the extent of tumors, these imaging modalities cannot adequately differentiate invasive lesions from edema, radiation necrosis, grading or gliosis. PET and SPECT can be used to localize and characterize tumors by measuring metabolic activity.

Due to favorable physical characteristics as well as extremely low price ($0.21/mCi), $^{99m}$Tc has been preferred to label radiopharmaceuticals. Although it has been reported that DTPA-drug conjugate could be labeled with $^{99m}$Tc effectively[1], DTPA moiety does not chelate with $^{99m}$Tc as stable as with $^{111}$In[2].

Bis-aminoethanethiol tetradentate ligands, also called diaminodithiol compounds, are known to form very stable Tc(V)O-complexes on the basis of efficient binding of the oxotechnetium group to two thiolsulfur and two amine nitrogen atoms[3,4]. $^{99m}$Tc-L,L-ethylenedicysteine ($^{99m}$Tc-EC) is the most recent and successful example of $N_2S_2$ chelates[4-6]. EC, a new renal imaging agent, can be labeled with $^{99m}$Tc easily and efficiently with high radiochemical purity and stability and is excreted through kidney by active tubular transport[4-10]. Other applications of EC would be chelated with galium-68 (a positron emitter, t1/2=68 min) for PET and gadolinium, iron or manganese for magnetic resonance imaging (MRI). In this invention, we report the efficient synthesis of a series of new ligands conjugated with EC. Such ligands can be labeled with $^{99m}$Tc for functional imaging by SPECT.

**Tumor Folate Receptor Targeting**

The radiolabeled ligands, such as pentetreotide and vasoactive intestinal peptide, bind to cell receptors, some of which are overexpressed on tumor cells[11-15]. Since these ligands are not immunogenic and are cleared quickly from the plasma, receptor imaging would seem to be more promising compared to antibody imaging.

Folic acid as well as antifolates such as methotrexate enter into cells via high affinity folate receptors (glycosylphosphatidylinositol-linked membrane folate-binding protein) in addition to classical reduced-folate carrier system[16-18]. Folate receptors (FRs) are overexpressed on many neoplastic cell types (e.g. lung, breast, ovarian, cervical, colorectal, nasopharyngeal, renal adenocarcinomas, malign melanoma and ependymomas), but primarily expressed only several normal differentiated tissues (e.g. choroid plexus, placenta, thyroid and kidney)[17,19-25]. FRs have been used to deliver folate-conjugated protein toxins, drug/antisense oligonucleotides and liposomes into tumor cells overexpressing the folate receptors[26-31]. Furthermore, bispecific antibodies that contain anti-FR antibodies linked to anti-T cell receptor antibodies have been used to target T cells to FR-positive tumor cells and are currently in clinical trials for ovarian carcinomas[32-36]. Similarly, this property has been inspired to develop radiolabeled folate-conjugates, such as $^{67}$Ga-deferoxamine-folate and $^{111}$In-DTPA-folate for imaging of folate receptor positive tumors[37-40]. Results of limited in vitro and in vivo studies with these agents suggest that folate receptors could be a potential target for tumor imaging. In this invention, we developed a series of new folate receptor ligands. These ligands are $^{99m}$Tc-EC-folate, $^{99m}$Tc-EC-methotrexate ($^{99m}$Tc-EC-MTX), $^{99m}$Tc-EC-tomudex ($^{99m}$Tc-EC-TDX).

**Tumor Hypoxia Targeting**

Tumor cells are more sensitive to conventional radiation in the presence of oxygen than in its absence; even a small percentage of hypoxic cells within a tumor could limit the response to radiation[41-43]. Hypoxic radioresistance has been demonstrated in many animal tumors but only in few tumor types in humans[44-46]. The occurrence of hypoxia in human tumors, in most cases, has been inferred from histology findings and from animal tumor studies. *In vivo* demonstration of hypoxia requires tissue measurements with oxygen electrodes and the invasiveness of these techniques has limited their clinical application.

Misonidazole (MISO) is a hypoxic cell sensitizer, and labeling MISO with different radioisotopes (e.g., $^{18}F$, $^{123}I$, $^{99m}Tc$) may be useful for differentiating a hypoxic but metabolically active tumor from a well-oxygenated active tumor by PET or planar scintigraphy. [$^{18}F$]Fluoromisonidazole (FMISO) has been used with PET to evaluate tumor hypoxia. Recent studies have shown that PET, with its ability to monitor cell oxygen content through [$^{18}F$]FMISO, has a high potential to predict tumor response to radiation[47-52]. PET gives higher resolution without collimation, however, the cost of using PET isotopes in a clinical setting is prohibitive. Although labeling MISO with iodine was the choice, high uptake in thyroid tissue was observed. Therefore, it is desirable to develop compounds for planar scintigraphy that the isotope is less expensive and easily available in most major medical facilities. In this invention, we present the synthesis of $^{99m}Tc$-EC-2-nitroimidazole and $^{99m}Tc$-EC-metronidazole and demonstrate their potential use as tumor hypoxia markers.

**Peptide Imaging of Cancer**

Peptides and amino acids have been successfully used in imaging of various types of tumors[53-62]. Glutamic acid based peptide has been used as a drug carrier for cancer treatment[58-62]. It is known that glutamate moiety of folate degraded and formed polyglutamate *in vivo*. The polyglutamate is then re-conjugated to folate to form folyl polyglutamate, which is involved in glucose metabolism. Labeling glutamic acid peptide may be useful in differentiating the malignancy of the tumors. In this invention, we report the synthesis of EC-glutamic acid pentapeptide and evaluate its potential use in imaging tumors.

**Imaging Tumor Apoptotic Cells**

Apoptosis occurs during the treatment of cancer with chemotherapy and radiation[63-67]. Annexin V is known to bind to phosphotidylserin, which is overexpressed by tumor apoptotic cells[66,67]. Assessment of apoptosis by annexin V would be useful to evaluate the efficacy of therapy such as disease progression or regression. In this invention, we synthesize $^{99m}Tc$-EC-annexin V (EC-ANNEX) and evaluate its potential use in imaging tumors.

**Imaging Tumor Angiogenesis**

Angiogenesis is in part responsible for tumor growth and the development of metastasis. Antimitotic compounds are antiangiogenic and are known for their potential use as anticancer drugs. These compounds inhibit cell division during the mitotic phase of the cell cycle. During the biochemical process of cellular functions, such as cell division, cell motility, secretion, ciliary and flagellar movement, intracellular transport and the maintenance of cell shape, microtubules are involved. It is known that antimitotic compounds bind with high affinity to microtubule proteins (tubulin), disrupting microtubule assembly and causing mitotic arrest of the proliferating cells. Thus, antimitotic compounds are considered as microtubule inhibitors or as spindle poisons[68].

Many classes of antimitotic compounds control microtubule assembly-disassembly by binding to tubulin[68-72]. Compounds such as colchicinoids interact with tubulin on the colchicine binding sites and inhibit microtubule assembly[68-70]. Among colchicinoids, colchicine is an effective anti-inflammatory drug used to treat prophylaxis of acute gout. Colchicine also is used in chronic myelocytic leukemia. Although colchicinoids are potent against certain types of tumor growth, the clinical therapeutic potential is limited due to inability to separate the therapeutic and toxic effects[68]. However, colchicine may be useful as a biochemical tool to assess cellular functions. In this invention, we developed $^{99m}Tc$-EC-colchicine (EC-COL) for the assessment of biochemical process on tubulin functions.

**b. How it works**

Bis-aminoethanethiol tetradentate ligands are known to form very stable Tc(V)O-complexes on the basis of efficient binding of the oxotechnetium group to two thiolsulfur and two amine nitrogen atoms. $^{99m}$Tc-L,L-ethylenedicysteine ($^{99m}$Tc-EC) is the most recent and successful example of $N_2S_2$ chelates. We have developed a series of new ligands conjugated with EC. These ligands can be labeled with $^{99m}$Tc for functional imaging by SPECT so that a better tumor treatment response is expected. The ligands are stored in kit forms and can be used in the following catagories.

**A. Prediction of Therapeutic Response (Folate receptors targeting)**

We hypothesize that if tumor tissue has less or no uptake by a radiolabeled drug, then such a drug should not be used in cancer treatment to save time and money. Assessment of tumor folate receptors with labeled folate receptor ligands prior to chemotherapy would provide rational means of selecting patients for treatment with methotrexate or methotrexate analogues (e.g. tomudex). Such selection of patients would permit more accurate evaluation of antifolates, since their use is limited to the patients with folate receptor overexpression, who could potentially benefit from the drug. $^{99m}$Tc-EC-folate, $^{99m}$Tc-EC-methotrexate ($^{99m}$Tc-EC-MTX), $^{99m}$Tc-EC-tomudex ($^{99m}$Tc-EC-TDX) were developed. We plan to assess the tumor uptake count density ratios before and after treatment with MTX in MTX-sensitive and MTX-resistant animal models.

**B. Monitoring Tumor Response to Treatment**

**Imaging Tumor Apoptotic Cells**

Apoptosis occurs during the treatment of cancer with chemotherapy and radiation. Annexin V is known to bind to phosphotidylserin, which is overexpressed by tumor apoptotic cells. Assessment of apoptosis by annexin V would be useful to evaluate the efficacy of therapy such as disease progression or regression. Thus, $^{99m}$Tc-EC-annexin V (EC-ANNEX) was developed.

**Imaging Tumor Hypoxia**

The assessment of tumor hypoxia by an imaging modality prior to radiation therapy would provide rational means of selecting patients for treatment with radiosensitizers or bioreductive drugs (e.g.tirapazamine, mitomycin C). Such selection of patients would permit more accurate treatment patients with hypoxic tumors. In addition, tumor suppressor gene (P53) is associated with multiple drug resistance. To correlate the imaging findings with the overexpression of P53 by histopathology before and after chemotherapy would be useful in following-up tumor treatment response. $^{99m}$Tc-EC-2-nitroimidazole and $^{99m}$Tc-EC-metronidazole were developed.

**Imaging Tumor Angiogenesis**

Angiogenesis is in part responsible for tumor growth and the development of metastasis. Antimitotic compounds are antiangiogenic and are known for their potential use as anticancer drugs. These compounds inhibit cell division during the mitotic phase of the cell cycle. During the biochemical process of cellular functions, such as cell division, cell motility, secretion, ciliary and flagellar movement, intracellular transport and the maintenance of cell shape, microtubules are involved. It is known that antimitotic compounds bind with high affinity to microtubule proteins (tubulin), disrupting microtubule assembly and causing mitotic arrest of the proliferating cells. Thus, antimitotic compounds are considered as microtubule inhibitors or as spindle poisons. Colchicine, a potent antiangiogenic agent, is known to inhibit microtubule polymerization and cell arrest at metaphase. Colchicine (COL) may be useful as a biochemical tool to assess cellular functions. $^{99m}$Tc-EC-COL was then developed.

**C. Differential Diagnosis**

**Differentiation of Malignancies (Peptide Imaging of Cancer)**
Peptides and amino acids have been successfully used in imaging of various types of tumors. Imaging tumors using peptide may be able to differentiate the malignancy of the tumors, the grading of tumors and the status of staging. $^{99m}$Tc-EC-glutamic acid pentapeptide was developed.

**c. How it is an improvement over the way things were done before**
Among all the isotopes used in radionuclide imaging, $^{99m}$Tc is the least expensive isotope ($0.21/mCi). Almost all the hospitals with Radiology/Nuclear Medicine Departments in the world have a $^{99}$Mo /$^{99m}$Tc generator. In this invention we improved the chemistry so that the ligands could be labeled with $^{99m}$Tc. These ligands are functional imaging ligands. They can characterize tumors so that better treatment response is expected. All these precursors can be stored in kit forms.

**d/e. Experimental procedure**
The NMR and mass spectral analysis were conducted at the University of Texas Health Science Center (Houston, TX). Nuclear magnetic resonance (NMR) spectra were recorded on a GE GN-500 Spectrometer. The mass data were obtained by fast atom bombardment on a Kratos MS 50 instrument (England). Elemental analysis was performed at Galbraith Laboratories, Inc. (Knoxville, TN). $^{99m}$Tc-pertechnetate was obtained from a commercial $^{99}$Mo/$^{99m}$Tc generator (Ultratechnekow FM™, Mallinckrodt Diagnostica, Holland).

## EXAMPLE 1: TUMOR FOLATE RECEPTOR TARGETING

**Synthesis of EC**
EC was prepared in a two-step synthesis according to the previously described methods[73,74]. The precursor, L-thiazolidine-4-carboxylic acid, was synthesized (m.p. 195°, reported 196-197°). EC was then prepared (m.p. 237°, reported 251-253°). The structure was confirmed by $^1$H-NMR and fast-atom bombardment mass spectroscopy (FAB-MS).

**Synthesis of aminoethylamido analogue of methotrexate (MTX-$NH_2$)**
MTX (227 mg, 0.5 mmol) was dissolved in 1 ml of HCl solution (2N). The pH value was <3. To this stirred solution, 2 ml of water and 4 ml of N-ethoxycarbonyl-2-ethoxy-1,2-dihydroquinoline (EEDQ, 6.609% in methanol, 1 mmol) were added at room temperature. Ethylenediamine (EDA, 0.6 ml, 10 mmol) was added slowly. The reaction mixture was stirred overnight and the solvent was evaporated in vacuo. The raw solid material was washed with diethyl ether (10 ml), acetonitrile (10 ml) and 95% ethyl alcohol (50 ml) to remove the unreacted EEDQ and EDA. The product was then dried by lyophilization and used without further purification. The product weighed 210 mg (84.7% ) as a yellow powder. m.p. of product: 195-198 °C (dec, MTX); $^1$H-NMR ($D_2O$) δ 2.98-3.04 (d, 8H, -$(CH_2)_2CONH(CH_2)_2NH_2$), 4.16-4.71 (m, 6H, -$CH_2$-pteridinyl, aromatic-$NCH_3$, NH-CH-COOH glutamate), 6.63-6.64 (d, 2H, aromatic-CO), 7.51-7.53 (d, 2H. aromatic-N), 8.36 (s, 1H, pteridinyl). FAB MS m/z calcd for $C_{22}H_{28}N_{10}O_4(M)^+$ 496.515, found 496.835.

**Synthesis of aminoethylamido analogue of folate (Folate-$NH_2$)**
Folic acid dihydrate (1 g, 2.0 mmol) was added in 10 ml of water. The pH value was adjusted to 2 using HCl (2 N). To this stirred solution, N-ethoxycarbonyl-2-ethoxy-1,2-dihydroquinoline (EEDQ, 1 g in 10 ml methanol, 4.0 mmol) and ethylenediamine (EDA, 1.3 ml, 18 mmol) were added slowly. The reaction mixture was stirred overnight at room temperature. The solvent was evaporated in vacuo. The product was precipitated in methanol (50 ml) and further washed with acetone (100 ml) to remove the unreacted EEDQ and EDA. The product was then freeze-dried and used without further purification. Ninhydrin (2% in methanol) spray indicated the positivity of amino group. The product weighed 0.6 g (yield 60% ) as a yellow powder. m.p. of product: 250° (dec). $^1$H-NMR ($D_2O$) δ 1.97-2.27 (m, 2H, -$CH_2$ glutamate of folate), 3.05-3.40 (d, 6H, -$CH_2CONH(CH_2)_2NH_2$), 4.27-4.84 (m, 3H, -$CH_2$-pteridinyl, NH-CH-COOH

glutamate), 6.68-6.70 (d, 2H, aromatic-CO), 7.60-7.62 (d, 2H. aromatic-N), 8.44 (s, 1H, pteridinyl). FAB MS m/z calcd for $C_{21}H_{25}N_9O_5(M)^+$ 483, found 483.21.

**Synthesis of ethylenedicysteine-folate (EC-Folate)**

To dissolve EC, NaOH (2N, 0.1 ml) was added to a stirred solution of EC (114 mg, 0.425 mmol) in water (1.5 ml). To this colorless solution, sulfo-NHS (92.3 mg, 0.425 mmol) and EDC (81.5 mg, 0.425 mmol) were added. Folate-$NH_2$ (205 mg, 0.425 mmol) was then added. The mixture was stirred at room temperature for 24 hours. The mixture was dialyzed for 48 hours using Spectra/POR molecular porous membrane with molecule cut-off at 500 (Spectrum Medical Industries Inc., Houston, TX). After dialysis, the product was freeze dried. The product weighed 116 mg (yield 35%). m.p. 195° (dec); $^1$H-NMR ($D_2O$) δ 1.98-2.28 (m, 2H, -$CH_2$ glutamate of folate), 2.60-2.95 (m, 4H and -$CH_2$-SH of EC), 3.24-3.34 (m, 10H, -$CH_2$-CO, ethylenediamine of folate and ethylenediamine of EC), 4.27-4.77 (m, 5H, -$CH_2$-pteridinyl, NH-CH-COOH glutamate of folate and NH-CH-COOH of EC), 6.60-6.62 (d, 2H, aromatic-CO), 7.58-7.59 (d, 2H. aromatic-N), 8.59 (s, 1H, pteridinyl). Anal. calcd for $C_{29}H_{37}N_{11}S_2O_8\ Na_2(8H_2O)$, FAB MS m/z $(M)^+$ 777.3 (free of water). C, 37.79; H, 5.75; N, 16.72; S, 6.95. Found: m/z $(M)^+$ 777.7 (20), 489.4 (100). C, 37.40; H, 5.42; N, 15.43; S, 7.58.

**Radiolabeling of EC-folate and EC with $^{99m}$Tc**

Radiosynthesis of $^{99m}$Tc-EC-folate was achieved by adding required amount of $^{99m}$Tc-pertechnetate into home-made kit containing the lyophilized residue of EC-folate (3 mg), $SnCl_2$ (100 μg), $Na_2HPO_4$ (13.5 mg), ascorbic acid (0.5 mg) and NaEDTA (0.5 mg). Final pH of preparation was 7.4. $^{99m}$Tc-EC was also obtained by using home-made kit containing the lyophilized residue of EC (3 mg), $SnCl_2$ (100 μg), $Na_2HPO_4$ (13.5 mg), ascorbic acid (0.5 mg) and NaEDTA (0.5 mg) at pH 10. Final pH of preparation was then adjusted to 7.4. Radiochemical purity was determined by TLC (ITLC SG, Gelman Sciences, Ann Arbor, MI) eluted with, respectively, acetone (system A) and ammonium acetate (1M in water):methanol (4:1) (system B). From radio-TLC (Bioscan, Washington, DC) analysis, the radiochemical purity was >95% for both radiopharmaceuticals. Radio-TLC data were summarized in Table 1. Synthesis of $^{99m}$Tc-EC-folate is shown in Figure 1.

**Radiolabeling of EC-MTX and EC-TDX with $^{99m}$Tc**

Use the same method described for the synthesis of EC-folate, EC-MTX and EC-TDX were prepared. The labeling procedure is the same as described for the preparation of $^{99m}$Tc-EC-folate except EC-MTX and EC-TDX were used. Synthesis of $^{99m}$Tc-EC-MTX and $^{99m}$Tc-EC-TDX is shown in Figures 2 and 3.

**Stability assay of $^{99m}$Tc-EC-folate, $^{99m}$Tc-EC-MTX and $^{99m}$Tc-EC-TDX**

Stability of $^{99m}$Tc-EC-Folate, $^{99m}$Tc-EC-MTX and $^{99m}$Tc-EC-TDX was tested in serum samples. Briefly, 740 KBq of 1 mg $^{99m}$Tc-EC-Folate, $^{99m}$Tc-EC-MTX and $^{99m}$Tc-EC-TDX was incubated in dog serum (200 μl) at 37 °C for 4 hours. The serum samples was diluted with 50% methanol in water and radio-TLC repeated at 0.5, 2 and 4 hours as described above.

**Tissue distribution studies**

Female Fischer 344 rats (150±25 g) (Harlan Sprague-Dawley, Indianapolis, IN) were inoculated subcutaneously with 0.1 ml of mammary tumor cells from the 13762 tumor cell line suspension ($10^6$ cells/rat, a tumor cell line specific to Fischer rats) into the hind legs using 25-gauge needles. Studies performed 14 to 17 days after implantation when tumors reached approximately 1 cm diameter. Animals were anesthetized with ketamine (10-15 mg/rat, intraperitoneally) before each procedure.

In tissue distribution studies, each animal injected intravenously with 370-550 KBq of $^{99m}$Tc-EC-folate or $^{99m}$Tc-EC (n=3/time point). The injected mass of each ligand was 10 μg per rat. At 20 min, 1, 2 and 4 h following administration of the radiopharmaceuticals, the anesthetized animals were sacrificed and the tumor and selected tissues were excised, weighed and counted for radioactivity by a gamma counter (Packard

Instruments, Downers Grove, IL). The biodistribution of tracer in each sample was calculated as percentage of the injected dose per gram of tissue wet weight (%ID/g). Counts from a diluted sample of the original injectate were used for reference. Tumor/nontarget tissue count density ratios were calculated from the corresponding %ID/g values. Student-t test was used to assess the significance of differences between two groups.

In a separate experiment, blocking studies were performed to determine receptor-mediated process. In blocking studies, for $^{99m}$Tc-EC-folate was co-administrated (i.v.) with 50 and 150 μmol/kg folic acid to tumor bearing rats (n=3/group). Animals were killed 1 h post-injection and data was collected.

**Scintigraphic imaging and autoradiography studies**
Scintigraphic images, using a gamma camera (Siemens Medical Systems, Inc., Hoffman Estates, IL) equipped with low-energy, parallel-hole collimator, were obtained 0.5, 2 and 4 hrs after i.v. injection of 18.5 MBq of $^{99m}$Tc-labeled radiotracer.

Whole-body autoradiogram were obtained by a quantitative image analyzer (Cyclone Storage Phosphor System, Packard, Meridian, CT). Following i.v. injection of 37 MBq of $^{99m}$Tc-EC-folate, animal killed at 1 h and body was fixed in carboxymethyl cellulose (4%). The frozen body was mounted onto a cryostat (LKB 2250 cryomicrotome) and cut into 100 μm coronal sections. Each section was thawed and mounted on a slide. The slide was then placed in contact with multipurpose phosphor storage screen (MP, 7001480) and exposed for 15 h ($^{99m}$Tc-labeled). The phosphor screen was excited by a red laser and resulting blue light that is proportional with previously absorbed energy was recorded.

## EXAMPLE 2: TUMOR HYPOXIA TARGETING

**Synthesis of 2-(2-methyl-5-nitro-$^1$H-imidazolyl)ethylamine (amino analogue of metronidazole, MN-NH$_2$)**
Amino analogue of metronidazole was synthesized according to the previously described methods[75]. Briefly, metronidazole was converted to a mesylated analogue (m.p. 149-150°C, reported 153-154°C, TLC:ethyl acetate, Rf=0.45), yielded 75%. Mesylated metronidazole was then reacted with sodium azide to afford azido analogue (TLC:ethyl acetate, Rf=0.52), yielded 80%. The azido analogue was reduced by triphenyl phosphine and yielded (60%) the desired amino analogue (m.p. 190-192°C, reported 194-195°C, TLC:ethyl acetate, Rf=0.15). Ninhydrin (2% in methanol) spray indicated the positivity of amino group of MN-NH$_2$. The structure was confirmed by $^1$H-NMR and mass spectroscopy (FAB-MS) m/z 171($M^+H$,100).

**Synthesis of Ethylenedicysteine-Metronidazole (EC-MN)**
Sodium hydroxide (2N, 0.2 ml) was added to a stirred solution of EC (134 mg, 0.50 mmol) in water (5 ml). To this colorless solution, sulfo-NHS (217 mg, 1.0 mmol) and EDC (192 mg, 1.0 mmol) were added. MN-NH$_2$ dihydrochloride salt (340 mg, 2.0 mmol) was then added. The mixture was stirred at room temperature for 24 hours. The mixture was dialyzed for 48 hrs using Spectra/POR molecular porous membrane with cut-off at 500 (Spectrum Medical Industries Inc., Houston, TX). After dialysis, the product was frozen dried using lyophilizer (Labconco, Kansas City, MO). The product weighed 315 mg (yield 55%). $^1$H-NMR ($D_2O$) δ 2.93 (s, 6H, nitroimidazole-$\underline{CH_3}$), 2.60-2.95 (m, 4H and -$\underline{CH_2}$-SH of EC), 3.30-3.66 (m, 8H, ethylenediamine of EC and nitromidazole-$CH_2$-$\underline{CH_2}$-$NH_2$), 3.70-3.99 (t, 2H, NH-$\underline{CH}$-CO of EC), 5.05 (t, 4H, metronidazole-$\underline{CH_2}$-$CH_2$-$NH_2$) (s, 2H, nitroimidazole C=$\underline{CH}$). FAB MS m/z 572 ($M^+$, 20). The synthetic scheme of EC-MN is shown in Figure 7.

**Synthesis of 3-(2-nitro-$^1$H-imidazolyl)propylamine (amino analogue of nitroimidazole, NIM-NH$_2$)**
To a stirred mixture containing 2-nitroimidazole (1g, 8.34 mmol) and $Cs_2CO_3$ (2.9g, 8.90 mmol) in dimethylformaide (DMF, 50 ml), 1,3- ditosylpropane (3.84 g, 9.99 mmol) was added. The reaction was heated at 80°C for 3 hours. The solvent was evaporated under vacuum and the residue was suspended in

ethylacetate. The solid was filtered, the solvent was concentrated, loaded on a silica gel-packed column and eluted with hexane:ethylacetate (1:1). The product, 3-tosylpropyl-(2-nitroimidazole), was isolated (1.67g, 57.5%) with m.p. 108-111°C. $^1$H-NMR ($CDCl_3$) δ 2.23 (m, 2H), 2.48 (S, 3H), 4.06 (t, 2H, J=5.7Hz), 4.52 (t, 2H, J=6.8Hz), 7.09 (S, 1H), 7.24 (S, 1H), 7.40 (d, 2H, J=8.2Hz),7.77 (d, 2H, J=8.2Hz).

Tosylated 2-nitroimidazole (1.33g, 4.08 mmol) was then reacted with sodium azide (0.29 g, 4.49 mmol) in DMF (10 ml) at 100°C for 3 hours. After cooling, water (20 ml) was added and the product was extracted from ethylacetate (3x20 ml). The solvent was dried over $MgSO_4$ and evaporated to dryness to afford azido analogue (0.6 g, 75%, TLC: hexane:ethyl acetate; 1:1, Rf=0.42). $^1$H-NMR ($CDCl_3$) δ 2.14 (m, 2H), 3.41 (t, 2H, J=6.2Hz), 4.54 (t, 2H, J=6.9Hz), 7.17 (S, 2H).

The azido analogue (0.57 g, 2.90 mmol) was reduced by triphenyl phosphine (1.14 g, 4.35 mmol) in tetrahydrofuran (THF) at room temperature for 4 hours. Concentrate HCl (12 ml) was added and heated for additional 5 hours. The product was extracted from ethylacetate and water mixture. The ethylacetate was dried over $MgSO_4$ and evaporated to dryness to afford amine hydrochloride analogue (360 mg, 60%). Ninhydrin (2% in methanol) spray indicated the positivity of amino group of NIM-$NH_2$. $^1$H-NMR ($D_2O$) δ 2.29 (m, 2H), 3.13 (t, 2H, J=7.8Hz), 3.60 (br, 2H), 4.35 (t, 2H, J=7.4Hz), 7.50 (d, 1H, J=2.1Hz),7.63 (d, 1H, J=2.1Hz).

**Synthesis of ethylenedicysteine-nitroimidazole (EC-NIM)**

Sodium hydroxide (2N, 0.6 ml) was added to a stirred solution of EC (134 mg, 0.50 mmol) in water (2 ml). To this colorless solution, sulfo-NHS (260.6 mg, 1.2 mmol), EDC (230 mg, 1.2 mmol) and sodium hydroxide (2N, 1 ml) were added. NIM-$NH_2$ hydrochloride salt (206.6 mg, 1.0 mmol) was then added. The mixture was stirred at room temperature for 24 hours. The mixture was dialyzed for 48 hrs using Spectra/POR molecular porous membrane with cut-off at 500 (Spectrum Medical Industries Inc., Houston, TX). After dialysis, the product was frozen dried using lyophilizer (Labconco, Kansas City, MO). The product weighed 594.8 mg (yield 98%). The synthetic scheme of EC-NIM is shown in Figure 8A. The structure is confirmed by $^1$H-NMR ($D_2O$) (Figure 8B).

**Radiolabeling of EC-MN and EC-NIM with $^{99m}$Tc**

Radiosynthesis of $^{99m}$Tc-EC-MN and $^{99m}$Tc-EC-NIM were achieved by adding required amount of $^{99m}$Tc-pertechnetate into home-made kit containing the lyophilized residue of EC-MN or EC-NIM (3 mg), $SnCl_2$ (100 μg), $Na_2HPO_4$ (13.5 mg), ascorbic acid (0.5 mg) and NaEDTA (0.5 mg). Final pH of preparation was 7.4. Radiochemical purity was determined by TLC (ITLC SG, Gelman Sciences, Ann Arbor, MI) eluted with acetone (system A) and ammonium acetate (1M in water):methanol (4:1) (system B), respectively. From radio-TLC (Bioscan, Washington, DC) analysis, the radiochemical purity was >95% for both radiotracers.

**Synthesis of [$^{18}$F]FMISO and [$^{131}$I]IMISO**

[$^{18}$F]fluoride was produced by the cyclotron using proton irradiation of enriched $^{18}$O-water in a small-volume silver target. The tosyl MISO[75] (20 mg) was dissolved in acetonitrile (1.5 ml), added to the kryptofix-fluoride complex. After heating, hydrolysis and column purification, A yield of 25-40% (decay corrected) of pure product was isolated with the end of bombardment (EOB) at 60 min. HPLC was performed on a C-18 ODS-120T column, 4.6 x 25 mm (Waters Corp., Milford, Mass), with water/acetonitrile, (80/20), using a flow rate of 1 ml/min. The no-carrier-added product corresponded to the retention time (6.12 min) of the unlabeled FMISO under similar conditions. The radiochemical purity was greater than 99%. Under the UV detector (310 nm), there were no other impurities. The specific activity of [$^{18}$F]FMISO determined was 1 Ci/μmol based upon UV and radioactivity detection of a sample of known mass and radioactivity.

[$^{131}$I]IMISO was prepared using the same precursor[76], briefly, 5 mg of tosyl MISO was dissolved in acetonitrile (1 ml), and Na$^{131}$I (1 mCi in 0.1 ml IN NaOH) (Dupont New England Nuclear, Boston, MA)

was added. After heating and purification, the product (60-70% yield) was obtained. Radio-TLC indicated the Rf values of 0.01 for the final product using chloroform methanol (7:3) as an eluant.

**Stability assay of $^{99m}$Tc-EC-MN and $^{99m}$Tc-EC-NIM**

Stability of labeled $^{99m}$Tc-EC-MN and $^{99m}$Tc-EC-NIM were tested in serum samples. Briefly, 740 KBq of 1 mg $^{99m}$Tc- EC-MN and $^{99m}$Tc-EC-NIM were incubated in dog serum (200 µl) at 37 $^{0}$C for 4 hours. The serum samples were diluted with 50% methanol in water and radio-TLC repeated at 0.5, 2 and 4 hours as described above.

**Tissue distribution studies of $^{99m}$Tc-EC-MN**

Female Fischer 344 rats (150±25 g) (Harlan Sprague-Dawley, Indianapolis, IN) were inoculated subcutaneously with 0.1 ml of mammary tumor cells from the 13762 tumor cell line suspension ($10^6$ cells/rat, a tumor cell line specific to Fischer rats) into the hind legs using 25-gauge needles. Studies performed 14 to 17 days after implantation when tumors reached approximately 1 cm diameter. Rats were anesthetized with ketamine (10-15 mg/rat, intraperitoneally) before each procedure.

In tissue distribution studies, each animal was injected intravenously with 370-550 KBq of $^{99m}$Tc-EC-MN or $^{99m}$Tc-EC (n=3/time point). The injected mass of $^{99m}$Tc-EC-MN was 10 µg per rat. At 0.5, 2 and 4 hrs following administration of the radiotracers, the rats were sacrificed and the selected tissues were excised, weighed and counted for radioactivity. The biodistribution of tracer in each sample was calculated as percentage of the injected dose per gram of tissue wet weight (%ID/g). Tumor/nontarget tissue count density ratios were calculated from the corresponding %ID/g values. The data was compared to [$^{18}$F]FMISO and [$^{131}$I]IMISO using the same animal model. Student t-test was used to assess the significance of differences between groups.

**Scintigraphic imaging and autoradiography studies**

Scintigraphic images, using a gamma camera (Siemens Medical Systems, Inc., Hoffman Estates, IL) equipped with low-energy, parallel-hole collimator, were obtained 0.5, 2 and 4 hrs after i.v. injection of 18.5 MBq of each radiotracer.

Whole-body autoradiogram was obtained by a quantitative image analyzer (Cyclone Storage Phosphor System, Packard, Meridian, CT). Following i.v. injection of 37 MBq of $^{99m}$Tc-EC-MN, the animals were killed at 1 h and the body were fixed in carboxymethyl cellulose (4%) as previously described[52]. The frozen body was mounted onto a cryostat (LKB 2250 cryomicrotome) and cut into 100 µm coronal sections. Each section was thawed and mounted on a slide. The slide was then placed in contact with multipurpose phosphor storage screen (MP, 7001480) and exposed for 15 hrs.

To ascertain whether $^{99m}$Tc-EC-NIM could monitor tumor response to chemotherapy, a group of rats with tumor volume 1.5 cm and ovarian tumor-bearing mice were treated with paclitaxel (40 mg/kg/rat, 80mg/kg/mouse, i.v.) at one single dose. The image was taken on day 4 after paclitaxel treatment. Percent of injected dose per gram of tumor weight with or without treatment was determined.

**Polarographic oxygen microelectrode $pO_2$ measurements**

To confirm tumor hypoxia, intratumoral $pO_2$ measurements were performed using the Eppendorf computerized histographic system. Twenty to twenty-five $pO_2$ measurements along each of two to three linear tracks were performed at 0.4 mm intervals on each tumor (40-75 measurements total). Tumor $pO_2$ measurements were made on three tumor-bearing rats. Using an on-line computer system, the $pO_2$ measurements of each track were expressed as absolute values relative to the location of the measuring point along the track, and as the relative frequencies within a $pO_2$ histogram between 0 and 100 mmHg with a class width of 2.5 mm.

## EXAMPLE 3: PEPTIDE IMAGING OF CANCER

### Synthesis of Ethylenedicysteine-Pentaglutamate (EC-GAP)

Sodium hydroxide (1N, 1 ml) was added to a stirred solution of EC (200 mg, 0.75 mmol) in water (10 ml). To this colorless solution, sulfo-NHS (162 mg, 0.75 mmol) and EDC (143 mg, 0.75 mmol) were added. Pentaglutamate sodium salt (M.W. 750-1500, Sigma Chemical Company) (500 mg, 0.67 mmol) was then added. The mixture was stirred at room temperature for 24 hours. The mixture was dialyzed for 48 hrs using Spectra/POR molecular porous membrane with cut-off at 500 (Spectrum Medical Industries Inc., Houston, TX). After dialysis, the product was frozen dried using lyophilizer (Labconco, Kansas City, MO). The product in the salt form weighed 0.95 g. The synthetic scheme of EC-GAP is shown in Figure 16.

### Stability Assay of $^{99m}$Tc-EC-GAP

Radiolabeling of EC-GAP with $^{99m}$Tc was achieved using the same procedure described previously. The radiochemical purity was 100%. Stability of labeled $^{99m}$Tc-EC-GAP was tested in serum samples. Briefly, 740 KBq of 1 mg $^{99m}$Tc- EC-GAP was incubated in dog serum (200 μl) at 37 $^{0}$C for 4 hours. The serum samples were diluted with 50% methanol in water and radio-TLC repeated at 0.5, 2 and 4 hours as described above.

### Scintigraphic Imaging Studies

Scintigraphic images, using a gamma camera equipped with low-energy, parallel-hole collimator, were obtained 0.5, 2 and 4 hrs after i.v. injection of 18.5 MBq of each radiotracer.

## EXAMPLE 4: IMAGING TUMOR APOPTOTIC CELLS

### Synthesis of Ethylenedicysteine-Annexin V (EC-ANNEX)

Sodium bicarbonate (1N, 1 ml) was added to a stirred solution of EC (5 mg, 0.019 mmol). To this colorless solution, sulfo-NHS (4 mg, 0.019 mmol) and EDC (4 mg, 0.019 mmol) were added. Annexin V (M.W. 33 kD, human, Sigma Chemical Company) (0.3 mg) was then added. The mixture was stirred at room temperature for 24 hours. The mixture was dialyzed for 48 hrs using Spectra/POR molecular porous membrane with cut-off at 10,000 (Spectrum Medical Industries Inc., Houston, TX). After dialysis, the product was frozen dried using lyophilizer (Labconco, Kansas City, MO). The product in the salt form weighed 12 mg.

### Stability Assay of $^{99m}$Tc-EC-ANNEX

Radiolabeling of EC-ANNEX with $^{99m}$Tc was achieved using the same procedure described in EC-GAP. The radiochemical purity was 100%. Stability of labeled $^{99m}$Tc-EC-ANNEX was tested in serum samples. Briefly, 740 KBq of 1 mg $^{99m}$Tc- EC-ANNEX was incubated in dog serum (200 μl) at 37 $^{0}$C for 4 hours. The serum samples were diluted with 50% methanol in water and radio-TLC repeated at 0.5, 2 and 4 hours as described above.

### Scintigraphic Imaging Studies

Scintigraphic images, using a gamma camera equipped with low-energy, parallel-hole collimator, were obtained 0.5, 2 and 4 hrs after i.v. injection of 18.5 MBq of the radiotracer. The animal models used were breast, ovarian and sarcoma. Both breast and ovarian-tumor bearing rats are known to overexpress high apoptotic cells. The imaging studies were conducted on day 14 after tumor cell inoculation. To ascertain the tumor treatment response, the pre-imaged mice were administered paclitaxel (80 mg/Kg, iv, day 14) and the images were taken on day 18.

## EXAMPLE 5: IMAGING TUMOR ANGIOGENESIS

### Synthesis of (Amino Analogue of Colchcine, COL-$NH_2$)

Demethylated amino and hydroxy analogue of colchcine was synthesized according to the previously described methods[77]. Briefly, colchicine (4 g) was dissolved in 100 ml of water containing 25% sulfuric acid. The reaction mixture was heated for 5 hours at 100°C. The mixture was neutralized with sodium carbonate. The product was filtered and dried over freeze dryer, yielded 2.4 g (70%) of the desired amino analogue (m.p. 153-155°C, reported 155-157°C). Ninhydrin (2% in methanol) spray indicated the positivity of amino group of COL-$NH_2$. The structure was confirmed by $^1$H-NMR and mass spectroscopy (FAB-MS). $^1$H-NMR ($CDCl_3$)δ 8.09 (S, 1H), 7.51 (d, 1H, J=12 Hz), 7.30 (d, 1H, J=12Hz), 6.56 (S, 1H), 3.91 (S, 6H), 3.85 (m, 1H), 3.67 (S, 3H), 2.25-2.52 (m, 4H). m/z 308.2($M^+$,20), 307.2 (100).

### Synthesis of Ethylenedicysteine-Colchcine (EC-COL)

Sodium hydroxide (2N, 0.2 ml) was added to a stirred solution of EC (134 mg, 0.50 mmol) in water (5 ml). To this colorless solution, sulfo-NHS (217 mg, 1.0 mmol) and EDC (192 mg, 1.0 mmol) were added. COL-$NH_2$ (340 mg, 2.0 mmol) was then added. The mixture was stirred at room temperature for 24 hours. The mixture was dialyzed for 48 hrs using Spectra/POR molecular porous membrane with cut-off at 500 (Spectrum Medical Industries Inc., Houston, TX). After dialysis, the product was frozen dried using lyophilizer (Labconco, Kansas City, MO). The product weighed 315 mg (yield 55%). $^1$H-NMR ($D_2O$) δ 7.39 (S, 1H), 7.20 (d, 1H, J=12Hz), 7.03 (d, 1H, J=12Hz), 6.78 (S,1H), 4.25-4.40 (m, 1H), 3.87 (S, 3H, -$OCH_3$), 3.84 (S, 3H, -$OCH_3$), 3.53 (S, 3H, -$OCH_3$), 3.42-3.52 (m, 2H), 3.05-3.26 (m, 4H), 2.63-2.82 (m, 4H), 2.19-2.25 (m, 4H). FAB MS m/z 580 (sodium salt, 20). The synthetic scheme of EC-COL is shown in Figure 21.

### Radiolabeling of EC-COL and EC with $^{99m}$Tc

Radiosynthesis of $^{99m}$Tc-EC-COLwas achieved by adding required amount of $^{99m}$Tc-pertechnetate into home-made kit containing the lyophilized residue of EC-COL (5 mg), $SnCl_2$ (100 μg), $Na_2HPO_4$ (13.5 mg), ascorbic acid (0.5 mg) and NaEDTA (0.5 mg). Final pH of preparation was 7.4. $^{99m}$Tc-EC was also obtained by using home-made kit containing the lyophilized residue of EC (5 mg), $SnCl_2$ (100 μg), $Na_2HPO_4$ (13.5 mg), ascorbic acid (0.5 mg) and NaEDTA (0.5 mg) at pH 10. Final pH of preparation was then adjusted to 7.4. Radiochemical purity was determined by TLC (ITLC SG, Gelman Sciences, Ann Arbor, MI) eluted with ammonium acetate (1M in water):methanol (4:1). Radio-thin layer chromatography (TLC, Bioscan, Washington, DC) was used to analyze the radiochemical purity for both radiotracers.

**Stability Assay of $^{99m}$Tc-EC-COL**
Stability of labeled $^{99m}$Tc-EC-COL was tested in serum samples. Briefly, 740 KBq of 5 mg $^{99m}$Tc- EC-COL was incubated in the rabbinate serum (500 µl) at 37 °C for 4 hours. The serum samples was diluted with 50% methanol in water and radio-TLC repeated at 0.5, 2 and 4 hours as described above.

**Tissue Distribution Studies**
Female Fischer 344 rats (150±25 g) (Harlan Sprague-Dawley, Indianapolis, IN) were inoculated subcutaneously with 0.1 ml of mammary tumor cells from the 13762 tumor cell line suspension ($10^6$ cells/rat, a tumor cell line specific to Fischer rats) into the hind legs using 25-gauge needles. Studies performed 14 to 17 days after implantation when tumors reached approximately 1 cm diameter. Rats were anesthetized with ketamine (10-15 mg/rat, intraperitoneally) before each procedure.

In tissue distribution studies, each animal was injected intravenously with 370-550 KBq of $^{99m}$Tc-EC-COL or $^{99m}$Tc-EC (n=3/time point). The injected mass of $^{99m}$Tc-EC-COL was 10 µg per rat. At 0.5, 2 and 4 hrs following administration of the radiotracers, the rats were sacrificed and the selected tissues were excised, weighed and counted for radioactivity. The biodistribution of tracer in each sample was calculated as percentage of the injected dose per gram of tissue wet weight (%ID/g). Tumor/nontarget tissue count density ratios were calculated from the corresponding %ID/g values. Student t-test was used to assess the significance of differences between groups.

**Scintigraphic Imaging Studies**
Scintigraphic images, using a gamma camera (Siemens Medical Systems, Inc., Hoffman Estates, IL) equipped with low-energy, parallel-hole collimator, were obtained 0.5, 2 and 4 hrs after i.v. injection of 300 µCi of $^{99m}$Tc-EC-COL and $^{99m}$Tc-EC. Computer outlined region of interest (ROI) was used to quantitate (counts per pixel) the tumor uptake versus normal muscle uptake.

## RESULTS

### EXAMPLE 1: TUMOR FOLATE RECEPTOR TARGETING

**Chemistry and Stability of $^{99m}$Tc-EC-Folate**
A simple, fast and high yield aminoethylamido and EC analogues of folate, MTX and TDX were developed. The structures of these analogues were confirmed by NMR and mass spectroscopic analysis. Radiosynthesis of EC-folate with $^{99m}$Tc was achieved with high (>95%) radiochemical purity. $^{99m}$Tc-EC-folate was found to be stable at 20 min, 1, 2 and 4 hours in dog serum samples.

**Biodistribution of $^{99m}$Tc-EC-folate**
Biodistribution studies showed that tumor/blood count density ratios at 20 min-4 h gradually increased for $^{99m}$Tc-EC-folate, whereas these values decreased for $^{99m}$Tc-EC in the same time period (Figure 4). %ID/g uptake values, tumor/blood and tumor/muscle ratios for $^{99m}$Tc-EC-folate and $^{99m}$Tc-EC were given in Tables 2 and 3, respectively.

In blocking studies, tumor/muscle and tumor/blood count density ratios were significantly decreased ($p<0.01$) with folic acid co-administrations (Figure 5).

**Scintigraphic Imaging and Autoradiography Studies**
Scintigraphic images obtained at different time points showed visualization of tumor in $^{99m}$Tc-EC-folate injected group. Contrary, there was no apparent tumor uptake in $^{99m}$Tc-EC injected group (Figure 6). Both radiotracer showed evident kidney uptake in all images. Autoradiograms performed at 1 h after injection of $^{99m}$Tc-EC-folate clearly demonstrated tumor activity.

## EXAMPLE 2: TUMOR HYPOXIA TARGETING

### Radiosynthesis and stability of $^{99m}$Tc-EC-MN and $^{99m}$Tc-EC-NIM

Radiosynthesis of EC-MN and EC-NIM with $^{99m}$Tc were achieved with high (>95%) radiochemical purity Radiochemical yield was 100%. $^{99m}$Tc-EC-MN and $^{99m}$Tc-EC-NIM (Figure 13) were found to be stable at 0.5, 2 and 4 hrs in dog serum samples. There was no degradation products observed. Radiofluorination and radioiodination of MISO were achieved easily using the same precursor. In both labeled MISO analogues, the radiochemical purity was greater than 99%.

### In vivo tissue distribution studies

The tissue distribution of $^{99m}$Tc-EC-MN and $^{99m}$Tc-EC in the tumor-bearing rats is shown in Tables 3 and 4. Due to high affinity for ionic $^{99m}$Tc, there was no significant and consistent thyroid uptake, suggesting the in vivo stability of $^{99m}$Tc-EC-MN (Table 4).

Biodistribution studies showed that tumor/blood and tumor/muscle count density ratios at 0.5-4 hr gradually increased for $^{99m}$Tc-EC-MN, [$^{18}$F]FMISO and [$^{131}$I]IMISO, whereas these values did not alter for $^{99m}$Tc-EC in the same time period (Figures 9 and 10). [$^{18}$F]FMISO showed the highest tumor-to-blood uptake ratio than those with [$^{131}$I]IMISO and $^{99m}$Tc-EC-MN at 30 min, 2 and 4 hrs post-injection. Tumor/blood and tumor/muscle ratios for $^{99m}$Tc-EC-MN and [$^{131}$I]IMISO at 2 and 4 hrs postinjection were not significantly different ($p<0.05$).

### Scintigraphic imaging and autoradiographic studies

Scintigraphic images obtained at different time points showed visualization of tumor in $^{99m}$Tc-EC-MN and $^{99m}$Tc-EC-NIM groups. Contrary, there was no apparent tumor uptake in $^{99m}$Tc-EC injected group (Figure 11). Autoradiograms performed at 1 hr after injection of $^{99m}$Tc-EC-MN clearly demonstrated tumor activity (Figure 12). Compare to $^{99m}$Tc-EC-NM, $^{99m}$Tc-EC-NIM appeared to provide better scintigraphic images due to higher tumor-to-background ratios. In breast tumor-bearing rats, tumor uptake was markedly higher in $^{99m}$Tc-EC-NIM group compared to $^{99m}$Tc-EC (Figure 14A). Data obtained from percent of injected dose of $^{99m}$Tc-EC-NIM per gram of tumor weight indicated that a 25% decreased uptake in the rats treated with paclitaxel when compared to control group (Figure 14B).

In ovarian tumor-bearing mice, there was a decreased tumor uptake in mice treated with paclitaxel (Figures 15A and 15B). Similar results were observed in sarcoma-bearing (Figures 15C and 15D). Thus, $^{99m}$Tc-EC-NIM could be used to assess tumor response to paclitaxel treatment.

### Polarographic oxygen microelectrode $pO_2$ measurements

Intratumoral $pO_2$ measurements of tumors indicated the tumor oxygen tension ranged $4.6\pm1.4$ mmHg as compared to normal muscle of $35\pm10$ mmHg. The data indicate that the tumors are hypoxic.

## EXAMPLE 3. PEPTIDE IMAGING OF CANCER

### Stability Assay of $^{99m}$Tc-EC-GAP

$^{99m}$Tc-EC-GAP found to be stable at 0.5, 2 and 4 hrs in dog serum samples. There was no degradation products observed.

### Scintigraphic imaging studies

Scintigraphic images obtained at different time points showed visualization of tumor in $^{99m}$Tc-EC-GAP group. The optimum uptake is at 30min to 1 hour post-administration (Figure 17).

## EXAMPLE 4: IMAGING TUMOR APOPTOTIC CELLS

### Stability Assay of $^{99m}$Tc-EC-ANNEX

$^{99m}$Tc-EC-ANNEX found to be stable at 0.5, 2 and 4 hrs in dog serum samples. There was no degradation products observed.

### Scintigraphic imaging studies

Scintigraphic images obtained at different time points showed visualization of tumor in $^{99m}$Tc-EC-ANNEX group (Figures 18-20). The images indicated that highly apoptotic cells have more uptake of $^{99m}$Tc-EC-ANNEX. There was no marked difference of tumor uptake between pre- and post-paclitaxel treatment in the high apoptosis (ovarian tumor-bearing) group (Figures 19A, 19B) and in the low apoptosis (sarcoma tumor-bearing) group (Figure 20A, 20B).

## EXAMPLE 5. IMAGING TUMOR ANGIOGENESIS

### Radiosynthesis and stability of $^{99m}$Tc-EC-COL

Radiosynthesis of EC-COL with $^{99m}$Tc was achieved with high (>95%) radiochemical purity (Figure 2). $^{99m}$Tc-EC-COL was found to be stable at 0.5, 2 and 4 hrs in rabbit serum samples. There was no degradation products observed (Figure 22).

### In Vivo Biodistribution

*In vivo* biodistribution of $^{99m}$Tc-EC-COL and $^{99m}$Tc-EC in breast-tumor-bearing rats are shown in Tables 1 and 2. Tumor uptake value (%ID/g) of $^{99m}$Tc-EC-COL at 0.5, 2 and 4 hours was 0.436±0.089, 0.395±0.154 and 0.221±0.006 (Table 5), whereas those for $^{99m}$Tc-EC were 0.342±0.163, 0.115±0.002 and 0.097±0.005, respectively (Table 3). Increased tumor-to-blood (0.52 ± 0.12 to 0.72 ± 0.07) and tumor-to-muscle (3.47 ± 0.40 to 7.97 ± 0.93) ratios as a function of time were observed in $^{99m}$Tc-EC-COL group (Figure 23). Conversely, tumor-to-blood and tumor-to-muscle values showed time-dependent decrease with $^{99m}$Tc-EC when compared to $^{99m}$Tc-EC-COL group in the same time period (Figure 24).

### Gamma Scintigraphic Imaging of $^{99m}$Tc-EC-COL in Breast Tumor-Bearing Rats

In vivo imaging studies in three breast-tumor-bearing rats at 1 hour post-administration indicated that the tumor could be visualized well with $^{99m}$Tc-EC-COL group (Figure 25), whereas, less tumor uptake in the $^{99m}$Tc-EC group was observed (Figure 26) . Computer outlined region of interest (ROI) showed that tumor/background ratios in $^{99m}$Tc-EC-COL group were significantly higher than $^{99m}$Tc-EC group (Figure 27).

## CONCLUSION

All these ligands showed potential application in imaging tumors. Compare to all the ligands developed, our results suggest that ligands could be a good candidate for imaging tumors due to the reasonable tumor-to tissue ratios.

## REFERENCES

1. Mathias CJ, Hubers D, Trump DP, Wang S, Luo J, Waters DJ, Fuchs PL, Low PS, Green MA. Synthesis of Tc-99m-DTPA-folate and preliminary evaluation as a folate-receptor-targeted radiopharmaceutical (Abstract). J Nucl Med 1997 (Supplement); *38*:87P.
2. Goldsmith SJ. Receptor imaging: Competitive or complementary to antibody imaging. Sem Nucl Med 1997; *27*:85-93.
3. Davison A, Jones AG, Orvig C, Sohn M. A new class of oxotechnetium(+5) chelate complexes containing a $TcON_2S_2$ Core. Inorg Chem 1980; *20*:1629-1632.
4. Verbruggen AM, Nosco DL, Van Nerom CG, et al. Tc-99m-L,L-ethylenedicysteine: A renal imaging agent. I.Labelling and evaluation in animals. J Nucl Med 1992; *33*:551-557.

5. Van Nerom CG, Bormans GM, De Roo MJ, et al. First experience in healthy volunteers with Tc-99m-L,L-ethylenedicysteine, a new renal imaging agent. Eur J Nucl Med 1993; *20*:738-746.
6. Surma MJ, Wiewiora J, Liniecki J. Usefulness of Tc-99m-N,N'-ethylene-1-dicysteine complex for dynamic kidney investigations. Nucl Med Comm 1994; *15*:628-635.
7. Verbruggen A, Nosco D, Van Nerom C, Bormans G, Adriaens P, De Roo M. Evaluation of Tc-99m L,L-ethylenedicysteine as a potential alternative to Tc-99m MAG3. Eur J Nucl Med 1990; *16*:429.
8. Van Nerom C, Bormans G, Bauwens J, Vandecruys A, De Roo M, Verbruggen A. Comparative evaluation of Tc-99m L,L-ethylenedicysteine and Tc-99m MAG3 in volunteers. Eur J Nucl Med 1990; *16*:417.
9. Jamar F, Stoffel M, Van Nerom C, et al. Clinical evaluation of Tc-99m L,L-ethylenedicysteine, a new renal tracer, in transplanted patients. J Nucl Med 1993; *34*:129P.
10. Jamar F, Van Nerom C, Verbruggen A, et al. Clearance of the new tubular agent Tc-99m L,L-ethylenedicysteine: Estimation by a simplified method. J Nucl Med 1993; 34:129P.
11. Britton KE, Granowska M. Imaging of tumors, in tomography in nuclear medicine. Proceedings of an International Symposium, Vienna, Austria, IAEA, 1996; 91-105.
12. Krenning EP, Kwekkeboom DJ, Bakker WH, et al. Somatostatin receptor scintigraphy with [In-111-DTPA-D-Phe] and [I-123-Tyr]-octretide: The Rotterdam experience with more than 1000 patients. Eur J Nucl Med 1995; *7*:716-731.
13. Reubi JC, Krenning EP, Lamberts SWJ, et al. In vitro detection of somatostatin receptors in human tumors. Metabolism 1992; *41*:104-110 (suppl 2).
14. Goldsmith SJ, Macapinlac H, O'Brien JP. Somatostatin receptor imaging in lymphoma. Sem Nucl Med 1995; *25*:262-271.
15. Virgolini I, Raderer M, Kurtaran A. Vasoactive intestinal peptide (VIP) receptor imaging in the localization of intestinal adenocarcinomas and endocrine tumors. N Eng J Med 1994; *331*:1116-1121.
16. Westerhof GR, Jansen G, Emmerik NV, Kathmann I, Rijksen G, Jackman AL, Schornagel JH. Membrane transport of natural folates and antifolate compounds in murine L1210 leukemia cells: Role of carrier- and receptor-mediated transport systems. Cancer Res 1991; *51*:5507-5513.
17. Orr RB, Kreisler AR, Kamen BA. Similarity of folate receptor expression in UMSCC 38 cells to squamous cell carcinoma differentiation markers. J Natl Cancer Inst 1995; *87*:299-303.
18. Hsueh CT, Dolnick BJ. Altered folate-binding protein mRNA stability in KB cells grown in folate-deficient medium. Biochem Pharmacol 1993; *45*:2537-2545.
19. Weitman SD, Lark RH, Coney LR, et al. Distribution of folate GP38 in normal and malignant cell lines and tissues. Cancer Res 1992; *52*:3396-3400.
20. Campbell IG, Jones TA, Foulkes WD, Trowsdale J. Folate-binding protein is a marker for ovarian cancer. Cancer Res 1991; *51*:5329-5338.
21. Weitman SD, Weinberg AG, Coney LR, Zurawski VR, Jennings DS, Kamen BA. Cellular localization of the folate receptor: potential role in drug toxicity and folate homeostasis. Cancer Res 1992; *52*:6708-6711.
22. Holm J, Hansen SI, Hoier-Madsen M, Sondergaard K, Bzorek M. Folate receptor of human mammary adenocarcinoma. APMIS 1994; *102*:413-419.
23. Ross JF, Chaudhuri PK, Ratnam M. Differential regulation of folate receptor isoforms in normal and malignant tissue in vivo and in established cell lines. Cancer 1994; *73*:2432-2443.
24. Franklin WA, Waintrub M, Edwards D, Christensen K, Prendegrast P, Woods J, Bunn PA, Kolhouse JF. New anti-lung-cancer antibody cluster 12 reacts with human folate receptors present on adenocarcinoma. Int J Cancer-Supplement 1994; *8*:89-95.
25. Weitman SD, Frazier KM, Kamen BA. The folate receptor in central nervous system malignancies of childhood. J Neuro-Oncology 1994; *21*:107-112.
26. Ginobbi P, Geiser TA, Ombres D, Citro G. Folic acid-polylysine carrier improves efficacy of c-myc antisense oligonucleotides on human melanoma (M14) cells. Anticancer Res 1997; *17*:29-35.
27. Leamon CP, Low PS. Delivery of macromolecules into living cells: a method that exploits folate receptor endocytosis. Proc Natl Acad Sci 1991; *88*:5572-5576.

28. Leamon CP, Low PS. Cytotoxicity of momordin-folate conjugates in cultured human cells. J Biol Chem 1992; *267*:24966-24971.
29. Leamon CP, Pastan I, Low PS. Cytotoxicity of folate-pseudomonas exotoxin conjugates toward tumor cells. J Biol Chem 1993; *268*:24847-24854.
30. Lee RJ, Low PS. Delivery of liposomes into cultured KB cells via folate receptor-mediated endocytosis. J Biol Chem 1994; *269*:3198-3204.
31. Ginobbi P, Geiser TA, Ombres D, Citro G. Folic acid-polylysine carrier improves efficacy of c-myc antisense oligodeoxynucleotides on human melanoma (M14) cells. Anticancer Res 1997; *17*:29-35.
32. Canevari S, Miotti S, Bottero F, Valota O, Colnaghi MI. Ovarian carcinoma therapy with monoclonal antibodies. Hybridoma 1993; *12*:501-507.
33. Bolhuis RLH, Lamers CHJ, Goey HS, et al. Adoptive immunotherapy of ovarian carcinoma with Bs-MAb targeted lymphocytes. A multicenter study. Int J Cancer 1992; *7*:78-81.
34. Patrick TA, Kranz DM, van Dyke TA, Roy EJ. Folate receptors as potential therapeutic targets in choroid plexus tumors of SV40 transgenic mice. J Neurooncol 1997; *32*:111-123.
35. Coney LR, Mezzanzanica D, Sanborn D, Casalini P, Colnaghi MI, Zurawski VR. Chimeric murine-human antibodies directed against folate binding receptor are efficient mediators of ovarian carcinoma cell killing. Cancer Res 1994; *54*:2448-2455.
36. Kranz DM, Patrick TA, Brigle KE, Spinella MJ, Roy EJ. Conjugates of folate and anti-T-cell-receptor antibodies specifically target folate-receptor-positive tumor cells for lysis. Proc Natl Acad Sci 1995; *92*:9057-9061.
37. Mathias CJ, Wang S, Lee RJ, Waters DJ, Low PS, Green MA. Tumor-selective radiopharmaceutical targeting via receptor-mediated endocytosis of Gallium-67-deferoxamine-folate. J Nucl Med 1996; *37*:1003-1008.
38. Wang S, Luo J, Lantrip DA, Waters DJ, Mathias CJ, Green MA, Fuchs PL, Low PS. Design and synthesis of [$^{111}$In]DTPA-folate for use as a tumor-targeted radiopharmaceutical. Bioconjugate Chem 1997; *8*:673-679.
39. Wang S, Lee RJ, Mathias CJ, Green MA, Low PS. Synthesis, purification, and tumor cell uptake of Ga-67 deferoxamine-folate, a potential radiopharmaceutical for tumor imaging. Bioconjugate Chem 1996; *7*:56-62.
40. Mathias CJ, Wang S, Waters DJ, Turek JJ, Low PS, Green MA. Indium-111-DTPA-folate as a radiopharmaceutical for targeting tumor-associated folate binding protein (Abstract). J Nucl Med 1997 (Supplement) *38*:133P.
41. Hall J. The oxygen effect and reoxygenation. In E. J. Hall (ed.) Radiobiology for the radiobiologist, 3rd edition. J.B. Lippincott Co., Philadelphia, PA, 1988; 137-160.
42. Bush, S, Jenkins, RDT, Allt, WEC, Beale, FA, Bena, H, Dembo, AJ and Pringle, JF. Definitive evidence for hypoxic cells influencing cure in cancer therapy. Br J Cancer (Suppl. III) 1978; *37*:302-306.
43. Gray H, Conger AD, Elbert M, Morsney S and Scold OCA. The concentration of oxygen dissolved in tissues at the time of irradiation as a factor in radiotherapy. Br J Radiol 1953; *26*:638-648.
44. Dische. A review of hypoxic-cell radiosensitization. Int J Radiat Oncol Biol Phys 1991; *20*:147-152.
45. Gatenby A, Kessler HB, Rosenblum JS, Coia LR, Moldofsky PJ, Hartz WH and Broder GJ. Oxygen distribution in squamous cell carcinoma metastases and its relationship to outcome of radiation therapy. Int J Radiat Oncol Biol Phys 1988; *14*:831-838.
46. Nordsmark M. Overgaard J and Overgaard J. Pretreatment oxygenation predicts radiation response in advanced squamous cell carcinoma of the head and neck. Radiother Oncol 1996; *41*:31-39.
47. Koh W-J, Rasey JS, Evans ML, Grierson JR, Lewellen, TK, Graham MM, Krohn KA and Griffin TW. Imaging of hypoxia in human tumors with $^{18}$F fluoromisonidazole. Int J Radiat Oncol Biol Phys 1992; *22*:199-212.
48. Valk ET, Mathis CA, Prados MD, Gilbert JC and Budinger TF. Hypoxia in human gliomas: Demonstration by PET with [$^{18}$F]fluoromisonidazole. J Nucl Med 1992; *33*:2133-2137.
49. Martin V, Caldwell JH, Rasey JS, Grunbaum Z, Cerqueia M, and Krohn KA. Enhanced binding of the hypoxic cell marker [$^{18}$F]fluoromisonidazole in ischemic myocardium. J Nucl Med 1989; *30*:194-201.

50. Rasey S, Koh WJ, Grieson JR, Grunbaum Z and Krohn KA. Radiolabeled fluoromisonidazole as an imaging agent for tumor hypoxia. Int J Radiat Oncol Biol Phys 1989; *17*:985-991.
51. Rasey S, Nelson NJ, Chin L, Evans ML, and Grunbaum Z. Characterization of the binding of labeled fluoromisonidazole in cells in vitro. Radiat Res 1990; 122: 301-308.
52. Yang J, Wallace S, Cherif A, Li C, Gretzer MB, Kim EE, and Podoloff DA. Development of F-18-labeled fluoroerythronitroimidazole as a PET agent for imaging tumor hypoxia. Radiology 1995; *194*:795-800.
53. Wester HJ, Herz M, Weber W, Heiss P, Schmidtke RS, Schwaiger M and Stöcklin G. Synthesis and radiopharmacology of –*O*(2-[$^{18}$F]fluoroethyl)-L-Tyrosine for tumor imaging. J Nucl Med 1999; *40*:205-212.
54. Coenen HH, Stöcklin G. Evaluation of radiohalogenated amino acid analogues as potential tracers for PET and SPECT studies of protein synthesis. Radioisot Klinik Forschung 1988; *18*:402-440.
55. Raderer M, Becherer A, Kurtaran A, Angelberger P, Li S, Leimer M, Weinlaender G, Kornek G, Kletter K, Scheithauer W, Virgolini I. Comparison of Iodine-123-vasoactive intestinal peptide receptor scintigraphy and Indium-111 CFT-102 immunoscintigraphy. J Nucl Med 1996; *37*:1480-1487.
56. Lambert SW, Bakker WH, Reubi JC, Krenning EP. Somatostatin receptor imaging in vivo localization of tumors with a radiolabeled somatostatin analog. J Steroid Biochem Mol Biol 1990; *37*:1079-1082.
57. Bakker WH, Krenning EP, Breeman WA, Koper JW, Kooij PP, Reubi JC, Klijn JG, Visser TJ, Docter R, Lamberts SW. Receptor scintigraphy with a radioiodinated somatostatin analogue: radiolabeling, purification, biologic activity and in vivo application in animals. J Nucl Med 1990; *31*:1501-1509.
58. Stella VJ, Mathew AE. Derivatives of taxol, pharmaceutical compositions thereof and methods for preparation thereof. United States Patent 4,960,790; 1990; October 2.
59. Butterfield DE, Fuji DK, Ladd DL, Snow RA, Tan JS, Toner JL. Segmented chelating polymers as imaging and therapeutic agents. United States Patent 5,730,968; 1998; March 24.
60. Piper, JR, McCaleb GS, Montgomery JA. A synthetic approach to poly(glutamyl) conjugates of methotrexate. J Med Chem 1983; *26*:291-294.
61. Mochizuki E, Inaki Y, Takemoto K. Synthesis of polyglutamates containing 5-substituted uracil moieties. Nucleic Acids Res 1985; *16*:121-124.
62. Dickinson HR and Hiltner A. Biodegradation of poly(χ-amino acid) hydrogel. II. In vitro. J Biomed Mater Res 1981; *15*:591.
63. Lennon SV, Martin SJ, Cotter TG. Dose-dependent induction of apoptosis in human tumor cell lines by widely diverging stimuli. Cell Prolif 1991; *24*:203-214.
64. Abrams MJ, Juweid M, Tenkate CI. Technetium-99m-human polyclonal IgG radiolabeled via the hydrazino nicotinamide derivative for imaging focal sites of infection in rats. J Nucl Med 1990, *31*:2022-2028.
65. Blankenberg FG, Katsikis PD, Tait JF, et al. In vivo detection and imaging of phosphatidylserine expression during programmed cell death. Proc Natl Acad Sci USA 1998; *95*:6349-6354.
66. Blankenberg FG, Katsikis PD, Tait JF, Davis RE, Naumovski L, Ohtsuki K, Kopiwoda S, Abrams MJ and Strauss HW. Imaging of apoptosis (programmed cell death) with $^{99m}$Tc annexin V. J Nucl Med 1999; *40*:184-191.
67. Tait JF, Smith C. Site-specific mutagenesis of annexin V: role of residues from Arg-200 to Lys-207 in phospholipid binding. Arch Biochem Biophys 1991; *288*:141-144.
68. Lu MC. Antimitotic agents. In: Foye, WO. ed. Cancer chemotherapeutic agents. Washington, DC: American Chemical Society 1995; 345-368.
69. Goh EL, Pircher TJ, Lobie PE. Growth hormone promotion of tubulin polymerization stabilizes the microtubule network and protects against colchicine-induced apoptosis. Endocrinology 1998; *139*:4364-4372.
70. Wang TH, Wang HS, Ichijo H, Giannakakou P, Foster JS, Fojo T, Wimalasena J. Microtubule-interfering agents activate c-Jun N-terminal kinase/stress-activated protein kinase through both Ras and apoptosis signal-regulating kinase pathways. J Biol Chem 1998; *273*:4928-4936.

71. Rowinsky, EK, Cazenave LA, Donehower RC. Taxol: A novel investigational antimicrotubule agent. J Natl Cancer Institute 1990; *82*(15):1247-1259.
72. Imbert TF. Discovery of podophyllotoxins. Biochimie 1998; *80*:207-222.
73. Ratner S, Clarke HT. The action of formaldehyde upon cysteine. J Am Chem Soc 1937; 59:200-206.
74. Blondeau P, Berse C, Gravel D. Dimerization of an intermediate during the sodium in liquid ammonia reduction of L-thiazolidine-4-carboxylic acid. Can J Chem 1967; *45*:49-52.
75. Hay MP, Wilson WR, Moselen JW, Palmer BD and Denny WA. Hypoxia-selective antitumor agents. Bis(nitroimidazolyl)alkanecarboxamides: a new class of hypoxia-selective cytotoxins and hypoxic cell radiosensitizers. J Med Chem 1994; *37*:381-391.
76. Cherif A, Yang DJ, Tansey W, Kim EE, and Wallace S. Synthesis of [$^{18}$F]fluoromisonidazole. Pharm Res 1994; *11*:466-469.
77. Raffauf RF, Farren AL, Ullyot GE. Colchicine. Derivatives of trimethylcolchicinic acid. J Am Chem Soc 1953; *75*:5292-5294.

**TABLE 1**
**Rf Values Determined by Radio-TLC (ITLC-SG) Studies**

| | System A* | System B† |
|---|---|---|
| $^{99m}$Tc-EC-folate | 0 | 1(>95%) |
| $^{99m}$Tc-EC | 0 | 1(>95%) |
| Free $^{99m}$Tc | 1 | 1 |
| Reduced $^{99m}$Tc | 0 | 0 |

* Acetone
† Ammonium Acetate (1M in water):Methanol (4:1)

**TABLE 2**
**Biodistribution of $^{99m}$Tc-EC-folate in Breast Tumor-Bearing Rats**

| | % of injected $^{99m}$Tc-EC-folate dose per organ or tissue | | | |
|---|---|---|---|---|
| | 20 min | 1 h | 2 h | 4 h |
| Blood | 0.370±0.049 | 0.165±0.028 | 0.086±0.005 | 0.058±0.002 |
| Lung | 0.294±0.017 | 0.164±0.024 | 0.092±0.002 | 0.063±0.003 |
| Liver | 0.274±0.027 | 0.185±0.037 | 0.148±0.042 | 0.105±0.002 |
| Stomach | 0.130±0.002 | 0.557±0.389 | 0.118±0.093 | 0.073±0.065 |
| Kidney | 4.328±0.896 | 4.052±0.488 | 5.102±0.276 | 4.673±0.399 |
| Thyroid | 0.311±0.030 | 0.149±0.033 | 0.095±0.011 | 0.066±0.011 |
| Muscle | 0.058±0.004 | 0.0257±0.005 | 0.016±0.007 | 0.008±0.0005 |
| Intestine | 0.131±0.013 | 0.101±0.071 | 0.031±0.006 | 0.108±0.072 |
| Urine | 12.637±2.271 | 10.473±3.083 | 8.543±2.763 | 2.447±0.376 |
| Tumor | 0.298±0.033 | 0.147±0.026 | 0.106±0.029 | 0.071±0.006 |
| Tumor/Blood | 0.812±0.098 | 0.894±0.069 | 1.229±0.325 | 1.227±0.129 |
| Tumor/Muscle | 5.157±0.690 | 5.739±0.347 | 6.876±2.277 | 8.515±0.307 |

Values shown represent the mean±standard deviation of data from 3 animals.

**TABLE 3**
**Biodistribution of $^{99m}$Tc-EC in Breast Tumor-Bearing Rats**

| | % of injected $^{99m}$Tc-EC dose per organ or tissue | | | |
|---|---|---|---|---|
| | 20 min | 1 h | 2 h | 4 h |
| Blood | 0.435±0.029 | 0.273±0.039 | 0.211±0.001 | 0.149±0.008 |
| Lung | 0.272±0.019 | 0.187±0.029 | 0.144±0.002 | 0.120±0.012 |
| Liver | 0.508±0.062 | 0.367±0.006 | 0.286±0.073 | 0.234±0.016 |
| Stomach | 0.136±0.060 | 0.127±0.106 | 0.037±0.027 | 0.043±0.014 |
| Kidney | 7.914±0.896 | 8.991±0.268 | 9.116±0.053 | 7.834±1.018 |
| Thyroid | 0.219±0.036 | 0.229±0.118 | 0.106±0.003 | 0.083±0.005 |
| Muscle | 0.060±0.006 | 0.043±0.002 | 0.028±0.009 | 0.019±0.001 |
| Intestine | 0.173±0.029 | 0.787±0.106 | 0.401±0.093 | 0.103±0.009 |
| Urine | 9.124±0.808 | 11.045±6.158 | 13.192±4.505 | 8.693±2.981 |
| Tumor | 0.342±0.163 | 0.149±0.020 | 0.115±0.002 | 0.096±0.005 |
| Tumor/Blood | 0.776±0.322 | 0.544±0.004 | 0.546±0.010 | 0.649±0.005 |
| Tumor/Muscle | 5.841±3.253 | 3.414±0.325 | 4.425±1.397 | 5.093±0.223 |

Values shown represent the mean± standard deviation of data from 3 animals.

**TABLE 4.**
**Biodistribution of $^{99m}$Tc-EC-metronidazole conjugate in breast tumor bearing rats[1]**

| | 30 Min. | 2 Hour | 4 Hour |
|---|---|---|---|
| Blood | 1.46±0.73 | 1.19±0.34 | 0.76±0.14 |
| Lung | 0.79±0.39 | 0.73±0.02 | 0.52±0.07 |
| Liver | 0.83±0.36 | 0.91±0.11 | 0.87±0.09 |
| Spleen | 0.37±0.17 | 0.41±0.04 | 0.37±0.07 |
| Kidney | 4.30±1.07 | 5.84±0.43 | 6.39±0.48 |
| Muscle | 0.08±0.03 | 0.09±0.01 | 0.07±0.01 |
| Intestine | 0.27±0.12 | 0.39±0.24 | 0.22±0.05 |
| Thyroid | 0.51±0.16 | 0.51±0.09 | 0.41±0.02 |
| Tumor | 0.34±0.13 | 0.49±0.02 | 0.50±0.09 |

1. Each rat received $^{99m}$Tc-EC-metronidazole (10 μCi, iv). Each value is percent of injected dose per gram weight (n=3)/time interval. Each data represents mean of three measurements with standard deviation.

## Table 5. Biodistribution of $^{99m}$Tc-EC-Colchicine in Breast Tumor Bearing Rats

| | 30 Min. | 2 Hour | 4 Hour |
|---|---|---|---|
| **Blood** | 0.837 ± 0.072 | 0.606 ± 0.266 | 0.307 ± 0.022 |
| **Lung** | 0.636 ± 0.056 | 0.407 ± 0.151 | 0.194 ± 0.009 |
| **Liver** | 1.159 ± 0.095 | 1.051 ± 0.213 | 0.808 ± 0.084 |
| **Spleen** | 0.524 ± 0.086 | 0.559 ± 0.143 | 0.358 ± 0.032 |
| **Kidney** | 9.705 ± 0.608 | 14.065 ± 4.007 | 11.097 ± 0.108 |
| **Muscle** | 0.129 ± 0.040 | 0.071 ± 0.032 | 0.028 ± 0.004 |
| **Stomach** | 0.484 ± 0.386 | 0.342 ± 0.150 | 0.171 ± 0.123 |
| **Uterus** | 0.502 ± 0.326 | 0.343 ± 0.370 | 0.133 ± 0.014 |
| **Thyroid** | 3.907 ± 0.997 | 2.297 ± 0.711 | 1.709 ± 0.776 |
| **Tumor** | 0.436 ± 0.089 | 0.395 ± 0.154 | 0.221 ± 0.006 |

* Each rat received $^{99m}$Tc-EC-Colchicine (10 μCi, iv.). Each value is the percent of injected dose per gram tissue weight (n=3)/time interval. Each data represents mean of three measurements with standard deviation.

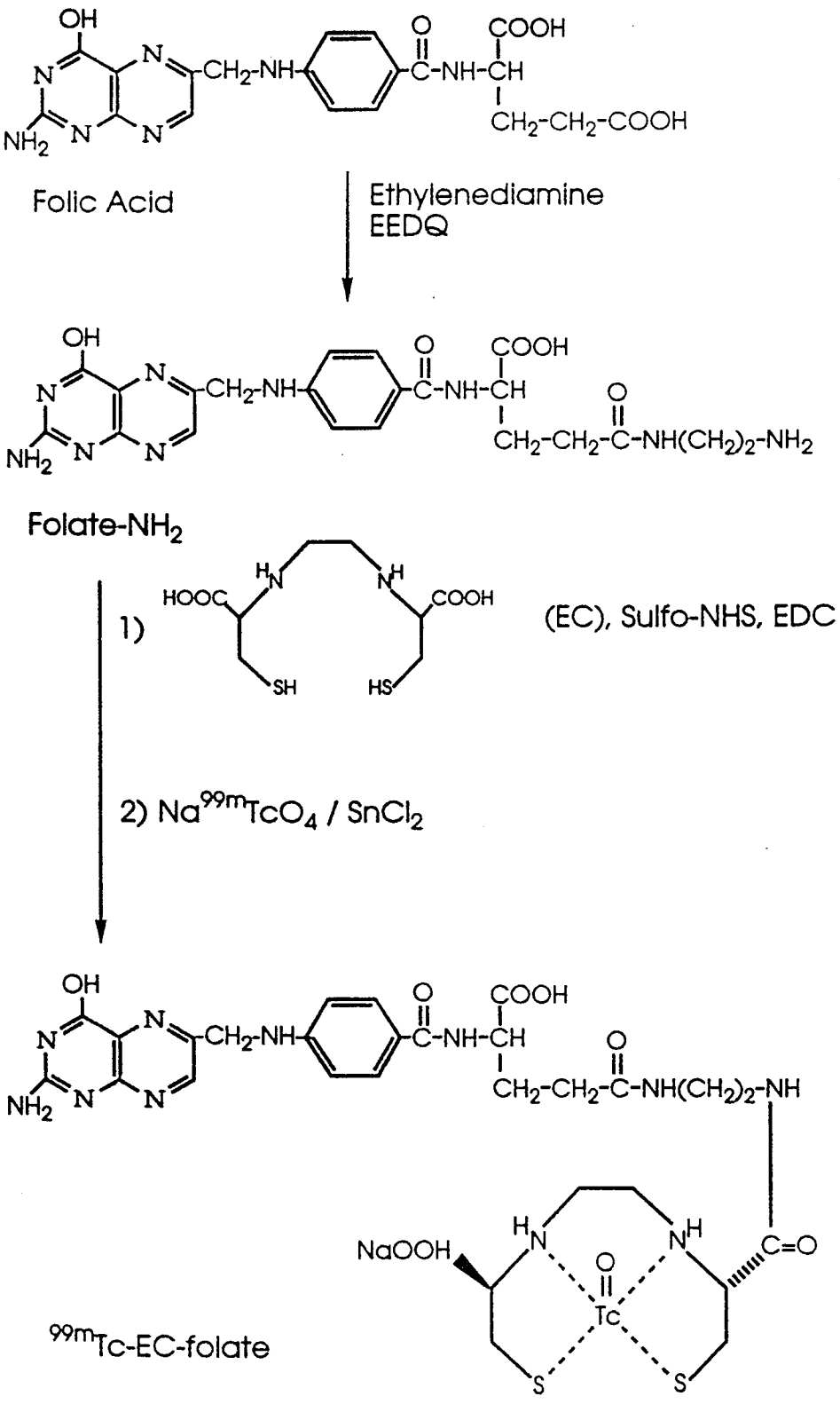


**Figure 1** Synthesis of $^{99m}$Tc-Ethylenedicysteine-folate ($^{99m}$Tc-EC-folate)

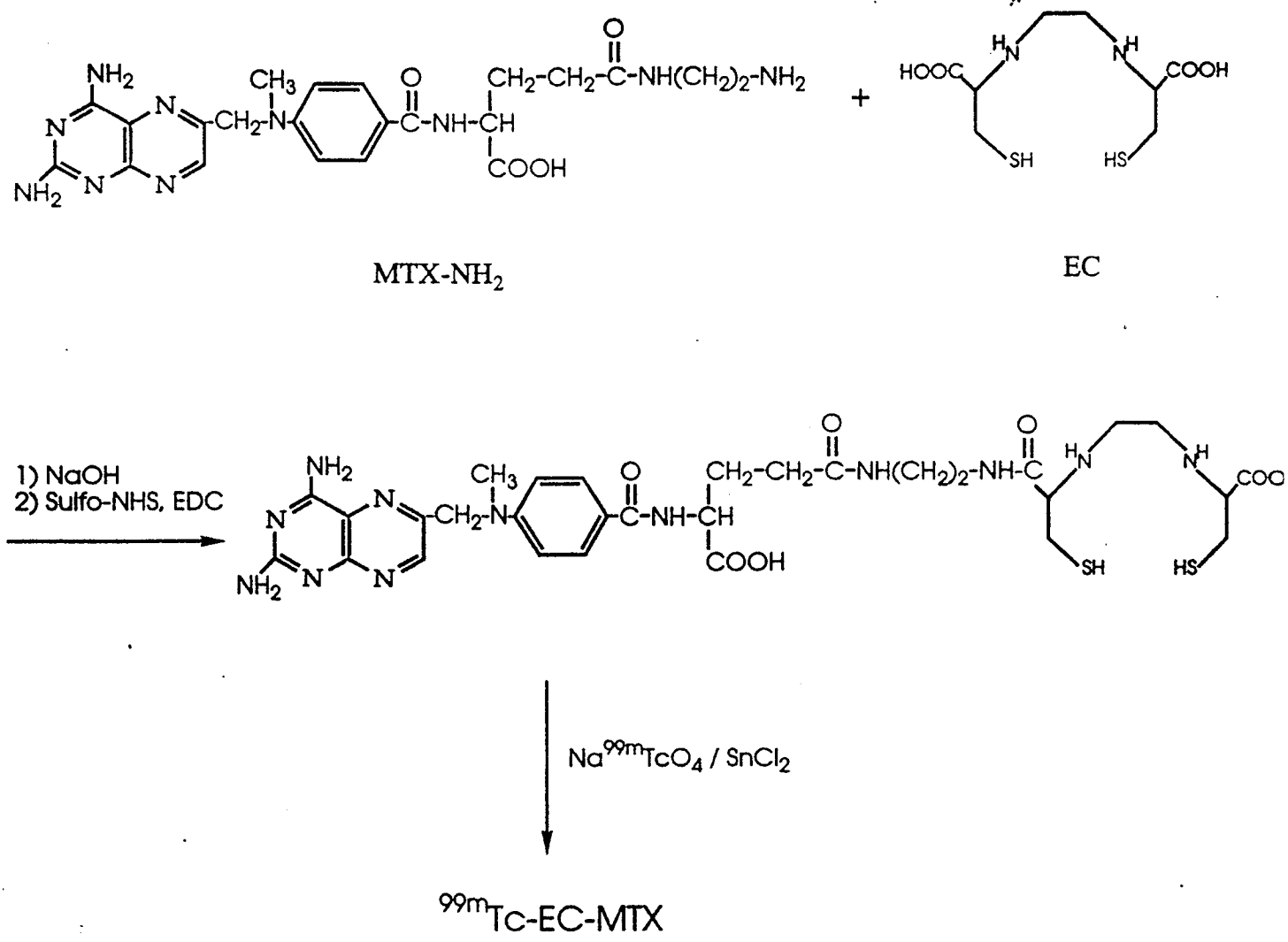


**Figure 2** . Synthesis $^{99m}$Tc-EC-methotrexate ($^{99m}$Tc-EC-methotrexate)

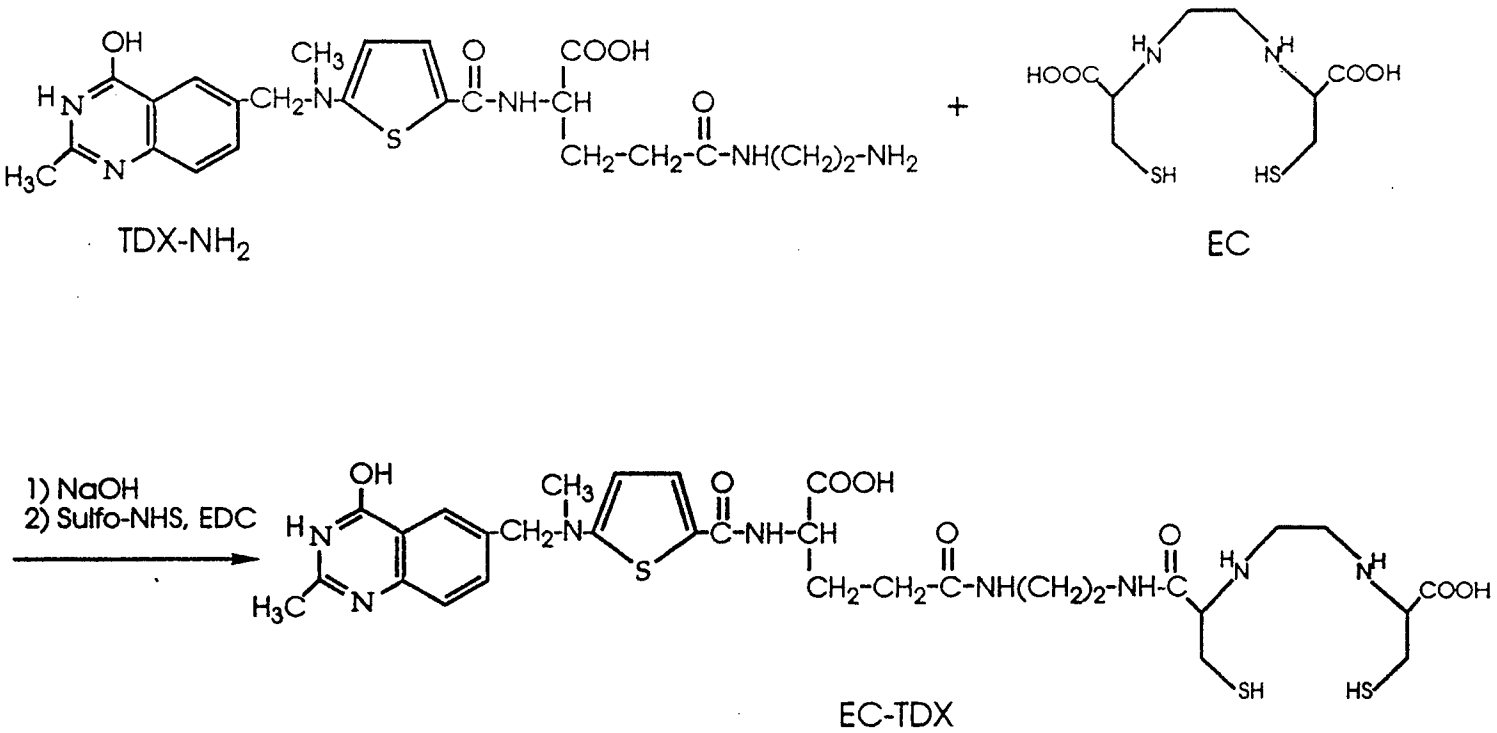


**Figure 3** . Synthesis of $^{99m}$Tc-EC-tomudex ($^{99m}$Tc-EC-TDX)

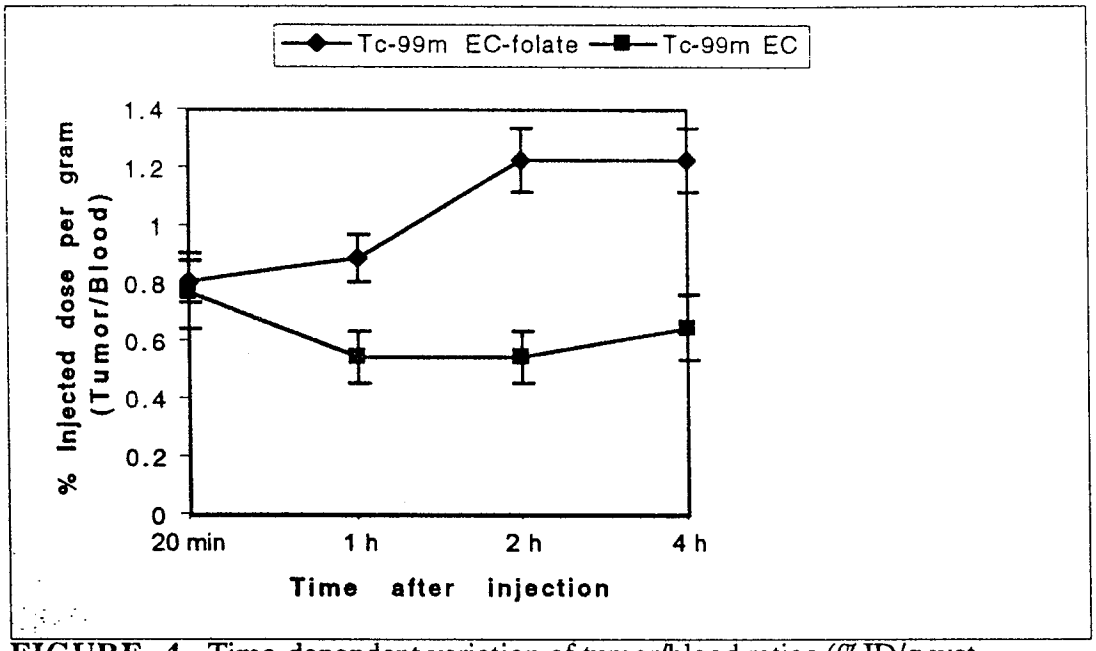


**FIGURE 4.** Time-dependent variation of tumor/blood ratios (%ID/g wet weight) for $^{99m}$Tc-EC-folate versus $^{99m}$Tc-EC (n=3/time point).

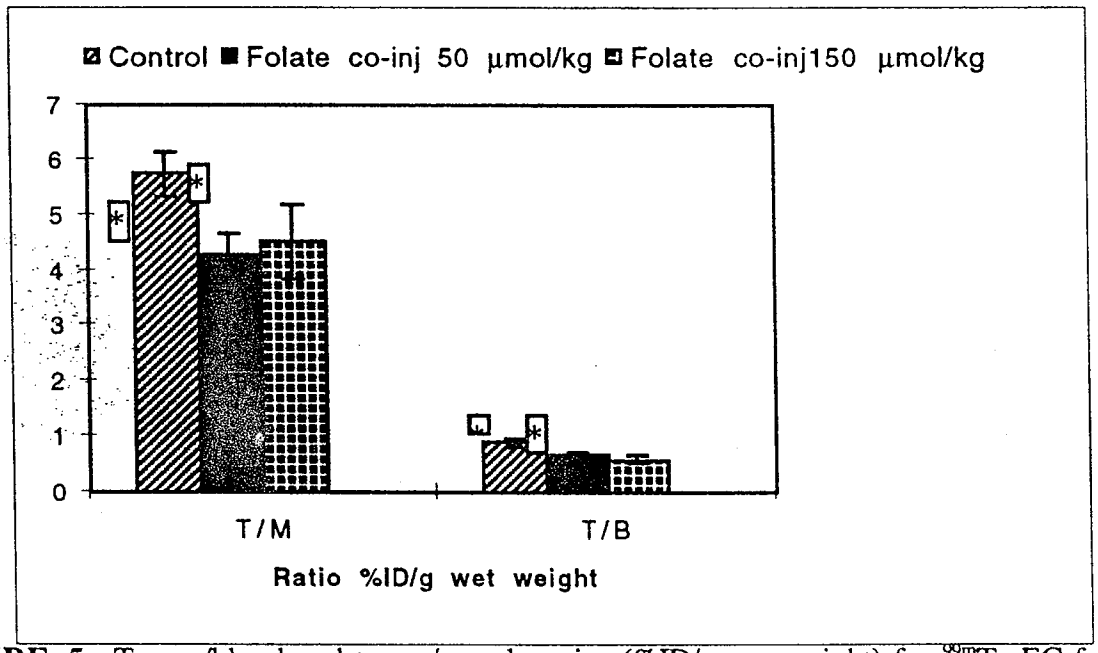


**FIGURE 5.** Tumor/blood and tumor/muscle ratios (%ID/g wet weight) for $^{99m}$Tc-EC-folate significantly decreased (* = $p<0.01$) with different doses of folate co-injections (n=3/group).

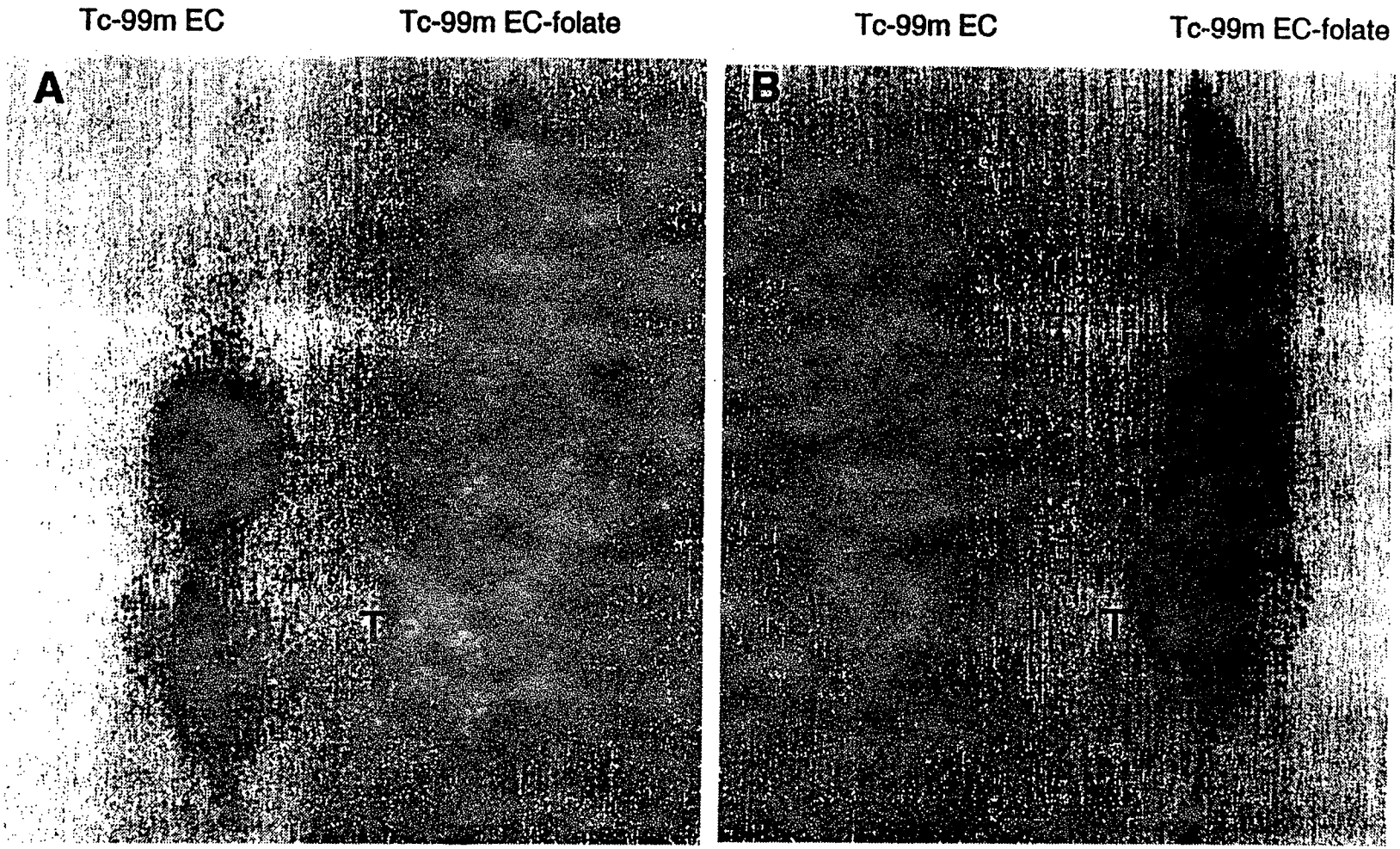


**Figure 6**. Selected gamma scintigraphy images (ventral view) of rats with a subcutaneous breast tumor in the right hind leg 1 (A) and 4 (B) hr following IV administration of $^{99m}$Tc-EC and $^{99m}$Tc-EC-folate. $^{99m}$Tc-EC-folate uptake was evident in the tumor (T) up to 4 hr. There was no apparent radiotracer uptake in the tumor area in $^{99m}$Tc-EC injected rat. Kidney and bladder activity were marked with both radiotracer. Tumor sizes were same (1 cm) in both animals.

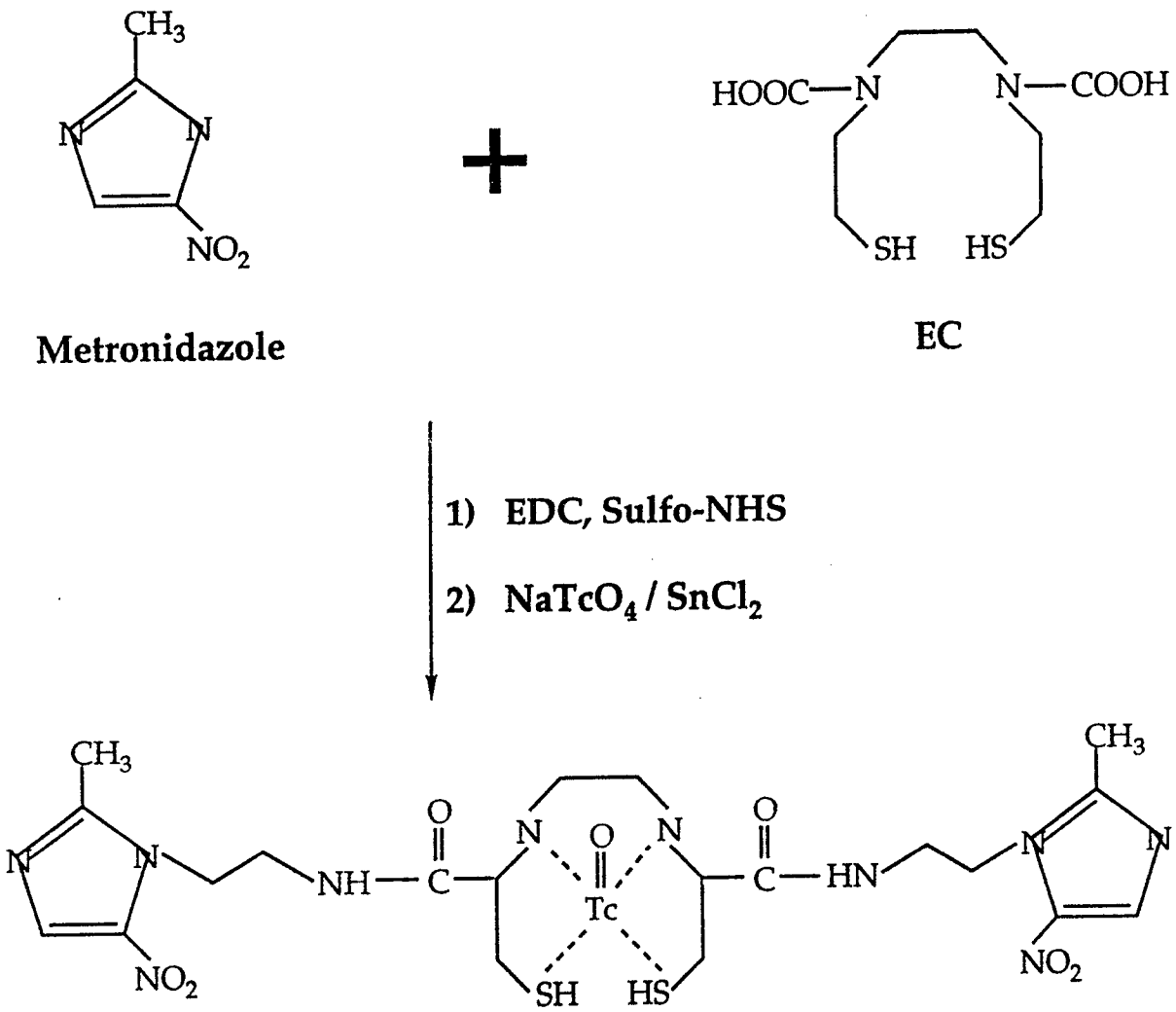




**Figure 7 . Radiosynthesis of $^{99m}$Tc-EC-metronidazole (EC-MN)**

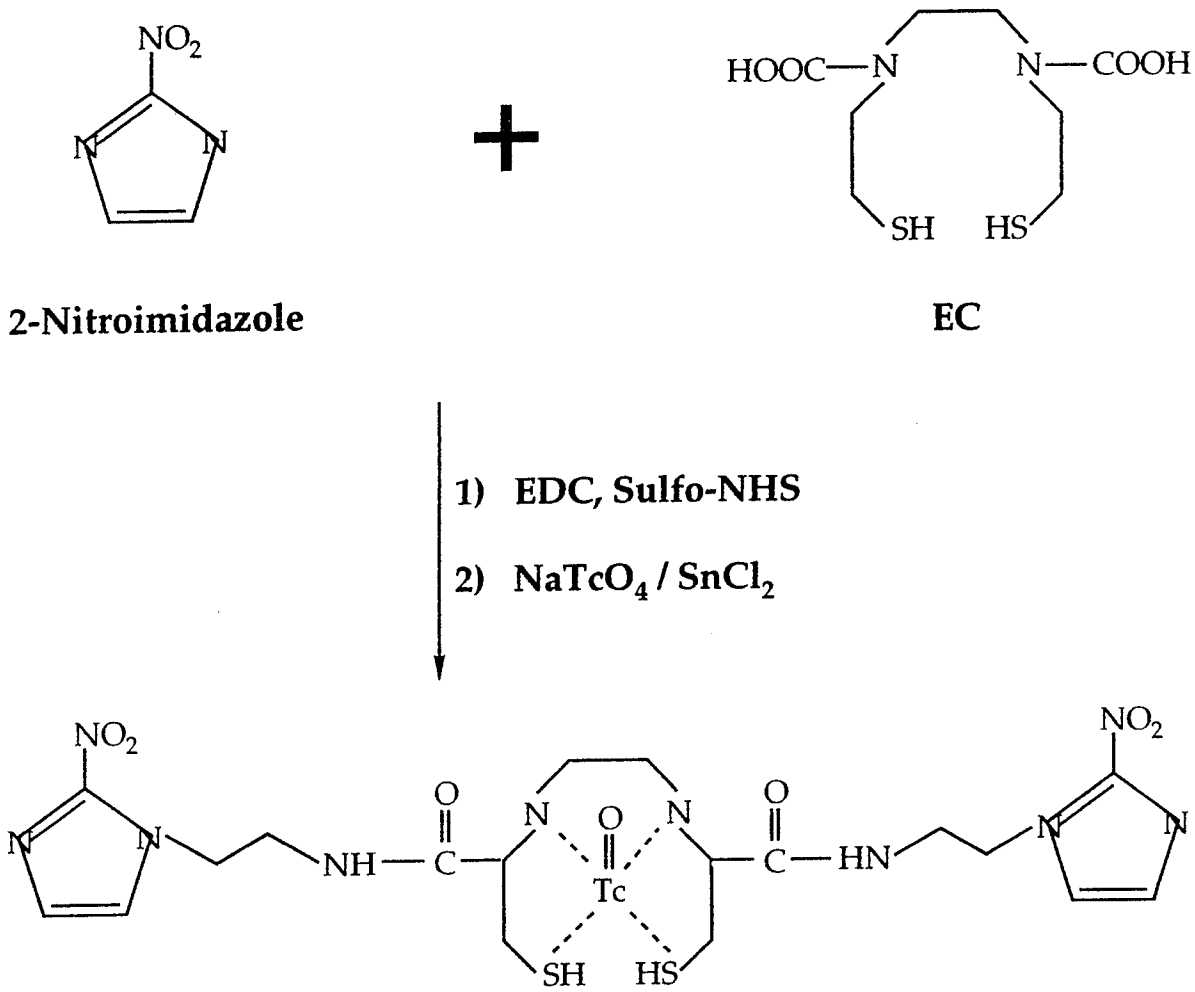


Figure 8A. Radiosynthesis of $^{99m}$Tc-EC-nitroimidazole (EC-NIM)

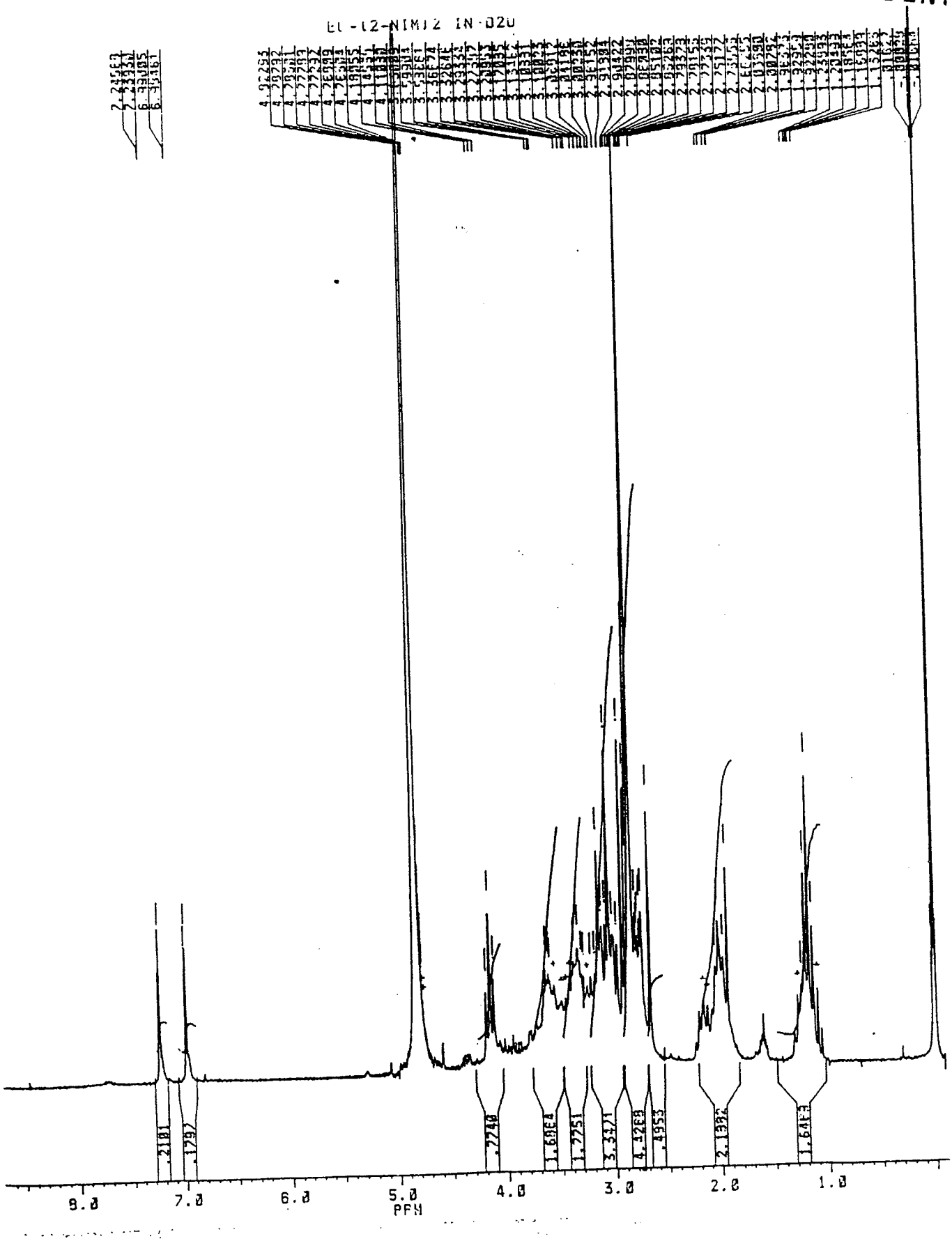


**Figure 8B.** Proton NMR spectrum of EC-nitroimidazole conjugate

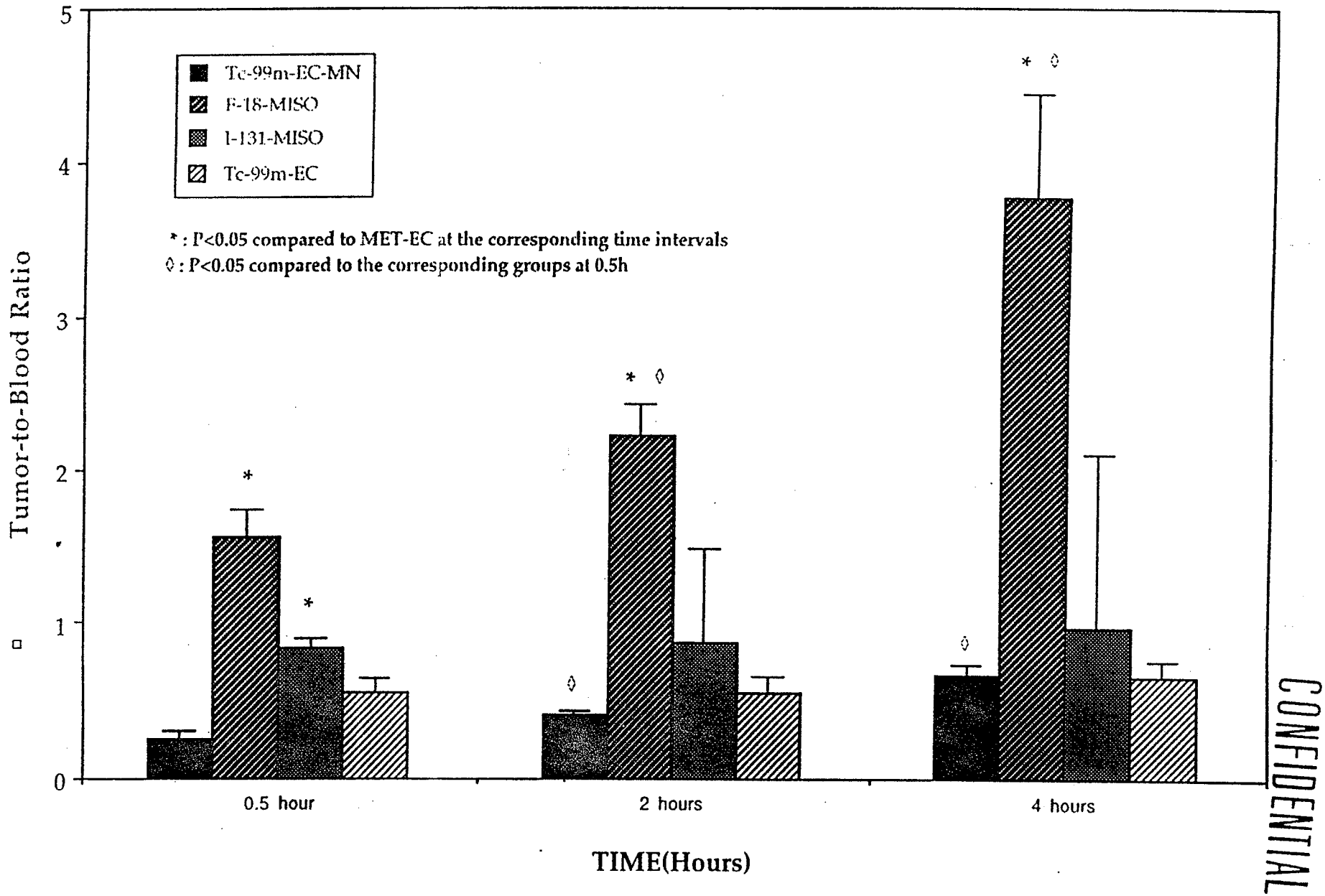


**Figure 9.** Time-dependent variation of tumor/blood uptake ratios (%ID/g wet weight) with $^{99m}$Tc-EC-MN, [$^{18}$F]FMISO, [$^{131}$I]IMISO versus $^{99m}$Tc-EC (n=3/time point).

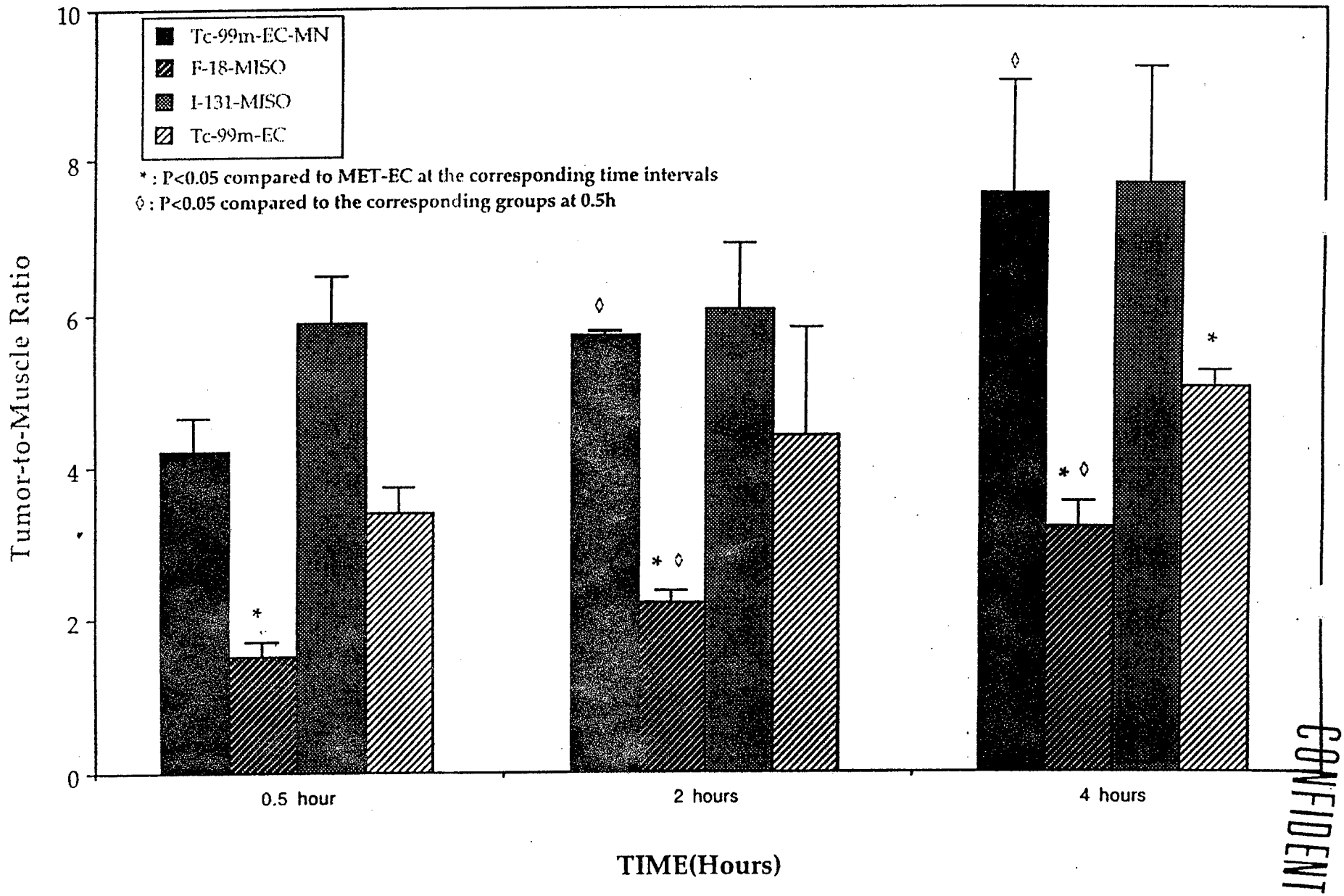


**Figure 10.** Time-dependent variation of tumor/muscle uptake ratios (%ID/g wet weight) with $^{99m}$Tc-EC-MN, [$^{18}$F]FMISO, [$^{131}$I]IMISO versus $^{99m}$Tc-EC (n=3/time point).

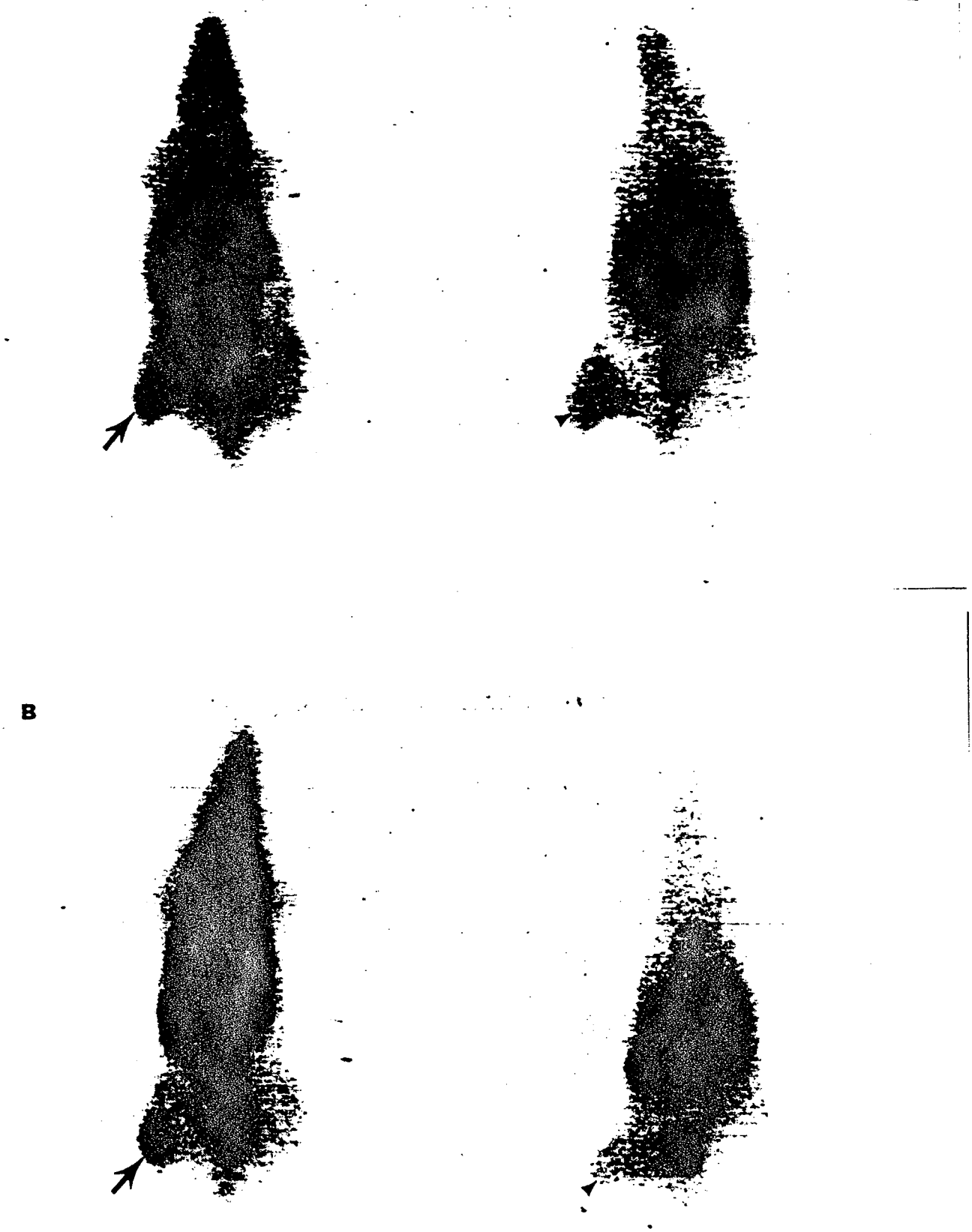


**Figure 11.** Selected gamma scintigraphy images (ventral view) of a rat with a subcutaneous breast tumor in the right hind leg at 1 (A) and 4 (B) hrs following intravenous administration of $^{99m}$Tc-EC-MN (left) and $^{99m}$Tc-EC (right). $^{99m}$Tc-EC-MN uptake was evident in the tumor (arrows) up to 4 hr. There was very minimal radiotracer uptake (arrowheads) in the tumor area with $^{99m}$Tc-EC.

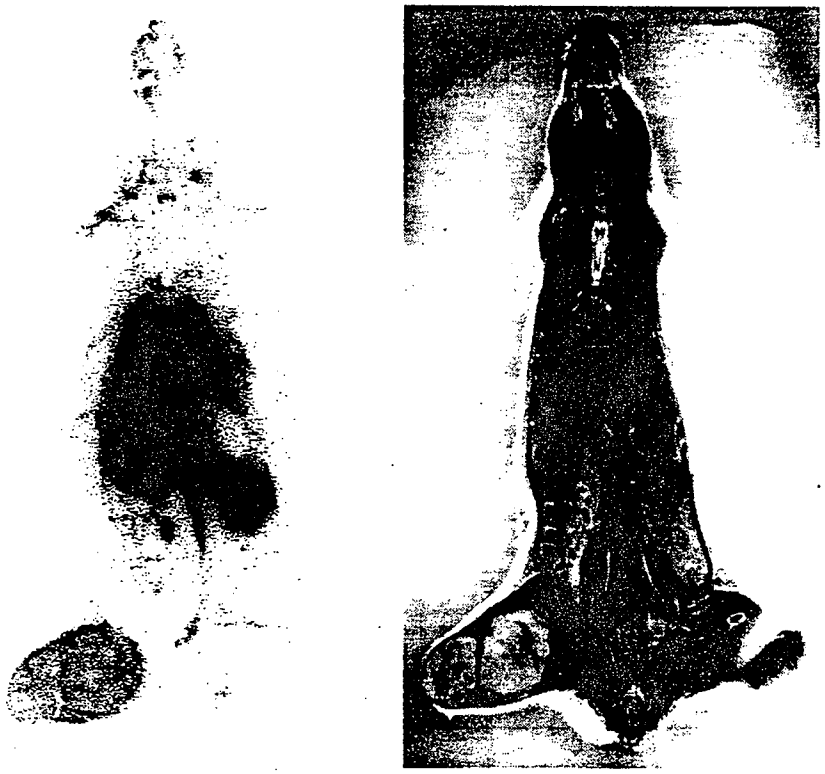

**Figure 12.** Whole-body autoradiogram (coronal section) obtained 30 min after intravenous injection of $^{99m}$Tc-EC-MN clearly demonstrated tumor activity. A corresponding sectional image is on the right.

SUMMARY REPORT
EC-(2-NIM)2 after adding serum 3:20

CONFIDENTIAL

Date: Start time: 16:02 Accum time: 00:00:50
Data File: Plate: 1 Lane: 1

Elect Resolution: NORMAL (Amp. Range: 0 - 2047)
Stop counts: 50000
Stop Counts Region: 0.00 to 20.00 cm
Rf Calculations: Origin: 1.50 cm Solvent Front: 19.00 cm
Integration Parameters: Auto Integration
Peak slope: 1.0 Min width: 0.1 Min %: 2.0

Total Count Region: 0.00cm to 20.00cm
Total Counts: 53170
Total CPM: 63810

| Reg. # | Start (cm) | Stop (cm) | Center (cm) | Rf | Region Counts | Region CPM | % of Tot Reg | % of Tot Cnt |
|---|---|---|---|---|---|---|---|---|
| 1 | 0.60 | 4.40 | 2.50 | 0.06 | 4557 | 5468 | 9.02 | 8.57 |
| 2 | 8.20 | 16.80 | 12.56 | 0.63 | 45980 | 55180 | 90.98 | 86.48 |
| TOTAL | | | | | 50540 | 60650 | 100.00 | 95.05 |

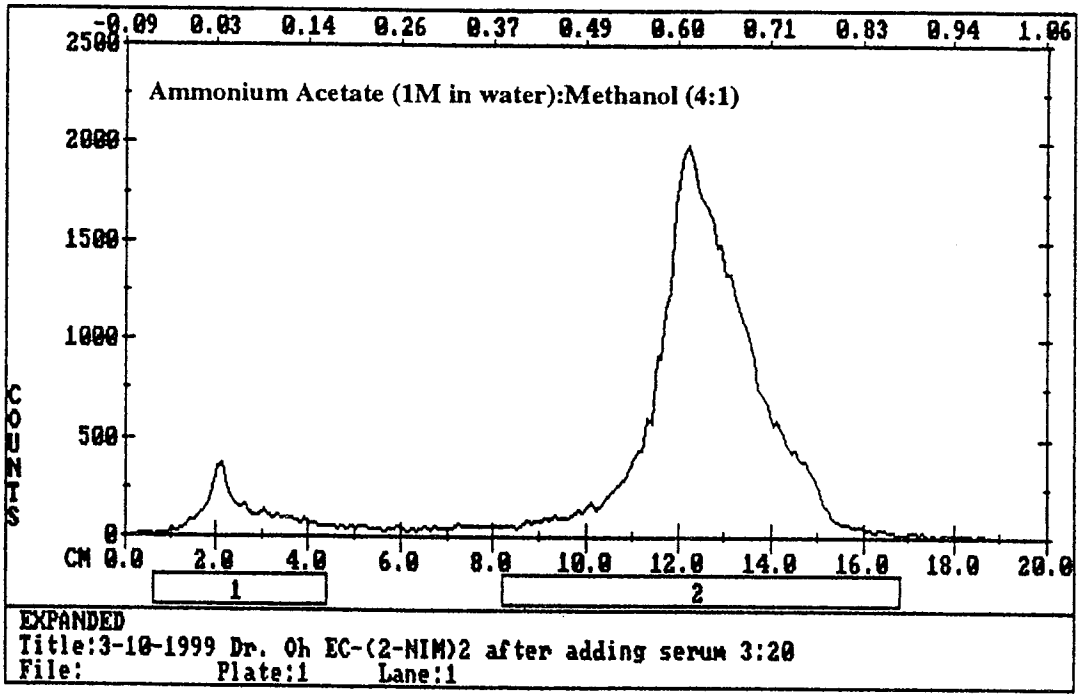


**Figure 13.** Radio-TLC analysis of $^{99m}$Tc-EC-nitronidazole (EC-NIM) in dog serum at 30 min.

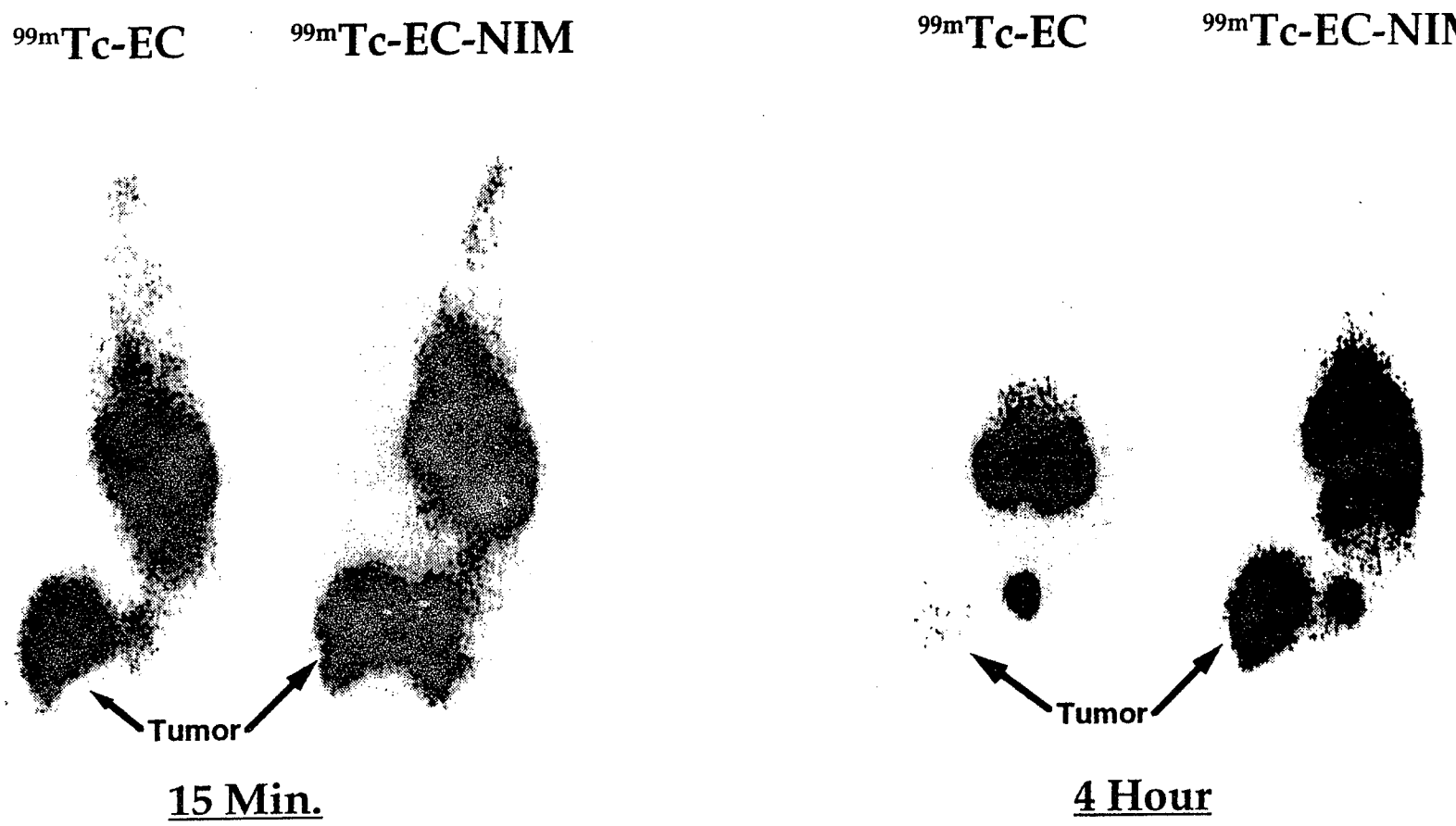




Figure 14A. Planar images of breast tumor-bearing rats following administration of $^{99m}$Tc-EC and $^{99m}$Tc-EC-NIM (300μCi/rat, iv., on day 14). Tumor uptake was higher in $^{99m}$Tc-EC-NIM when compared to $^{99m}$Tc-EC at 4 hours.

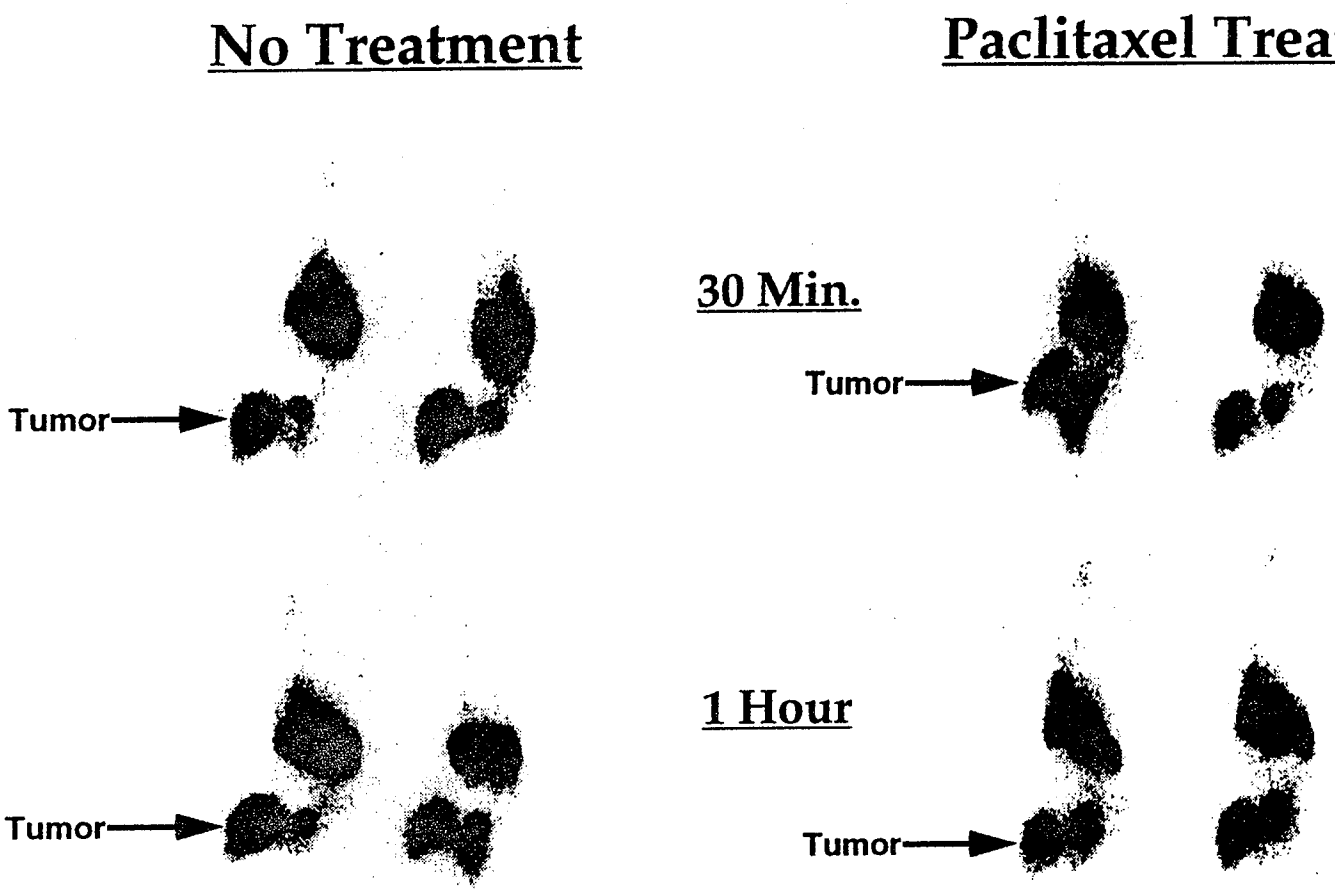


Figure 14B. Planar images of breast tumor-bearing rats without and with paclitaxel treatment (40mg/kg, iv., single injection on day 14) following the administration of $^{99m}$Tc-EC-NIM (300μCi/rat, iv.) on day 18 indicated that tumor volume and tumor uptake decreased after paclitaxel treatment.

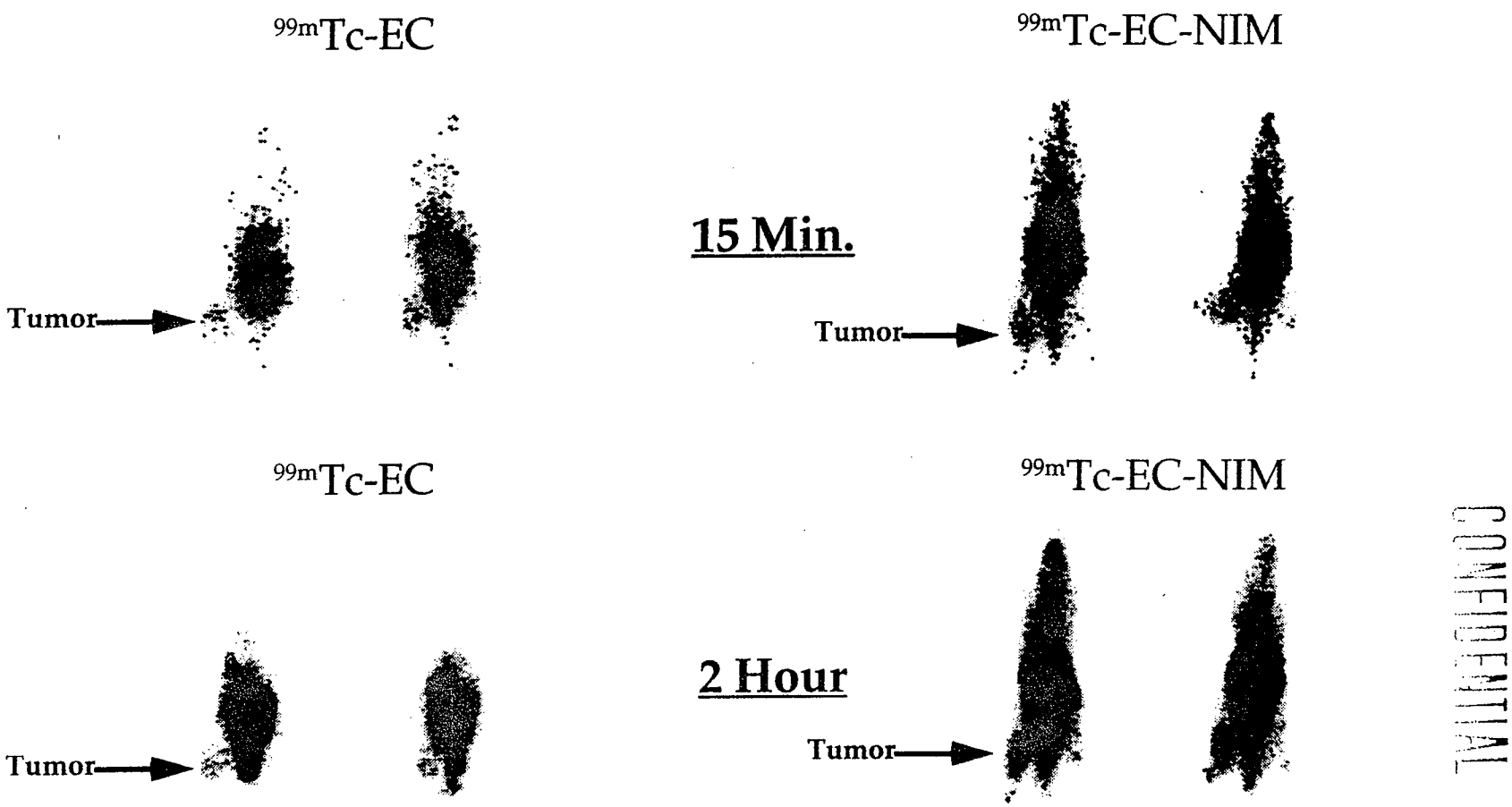




**Figure 15A.** **Planar images of ovarian (OCA-1) tumor-bearing mice after administration of $^{99m}$Tc-EC and $^{99m}$Tc-EC-NIM (100μCi/mouse, iv.) showed that the tumor could be visualized from 15 min. to 2 hours postinjection with $^{99m}$Tc-EC-NIM.**

## $^{99m}$Tc-EC-Nitroimidazole (NIM)
## (100μCi/mouse, iv.)

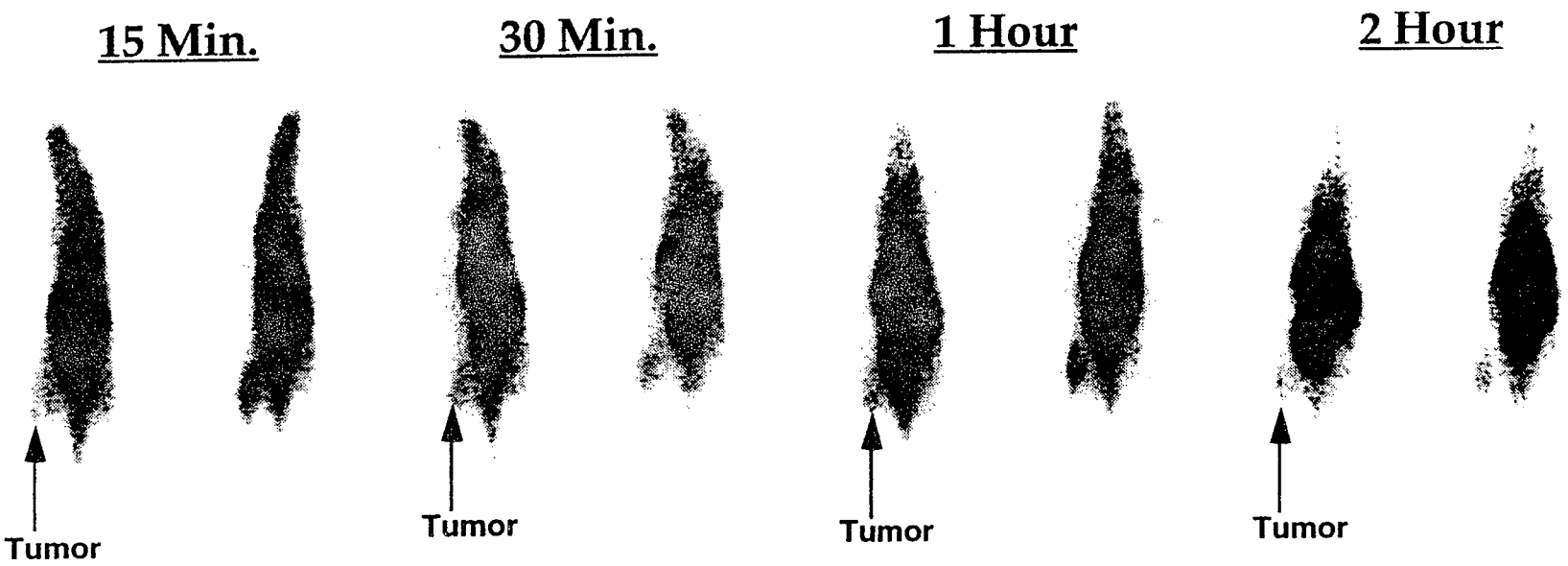


Figure 15B. On day 18, planar images of OCA-1 tumor-bearing mice (high apoptosis) after paclitaxel treatment (80mg/kg, iv., single injection on day 14) showed that the tumors had less uptake compared with the pretreatment data.

## $^{99m}$Tc-EC-Nitroimidazole (NIM)

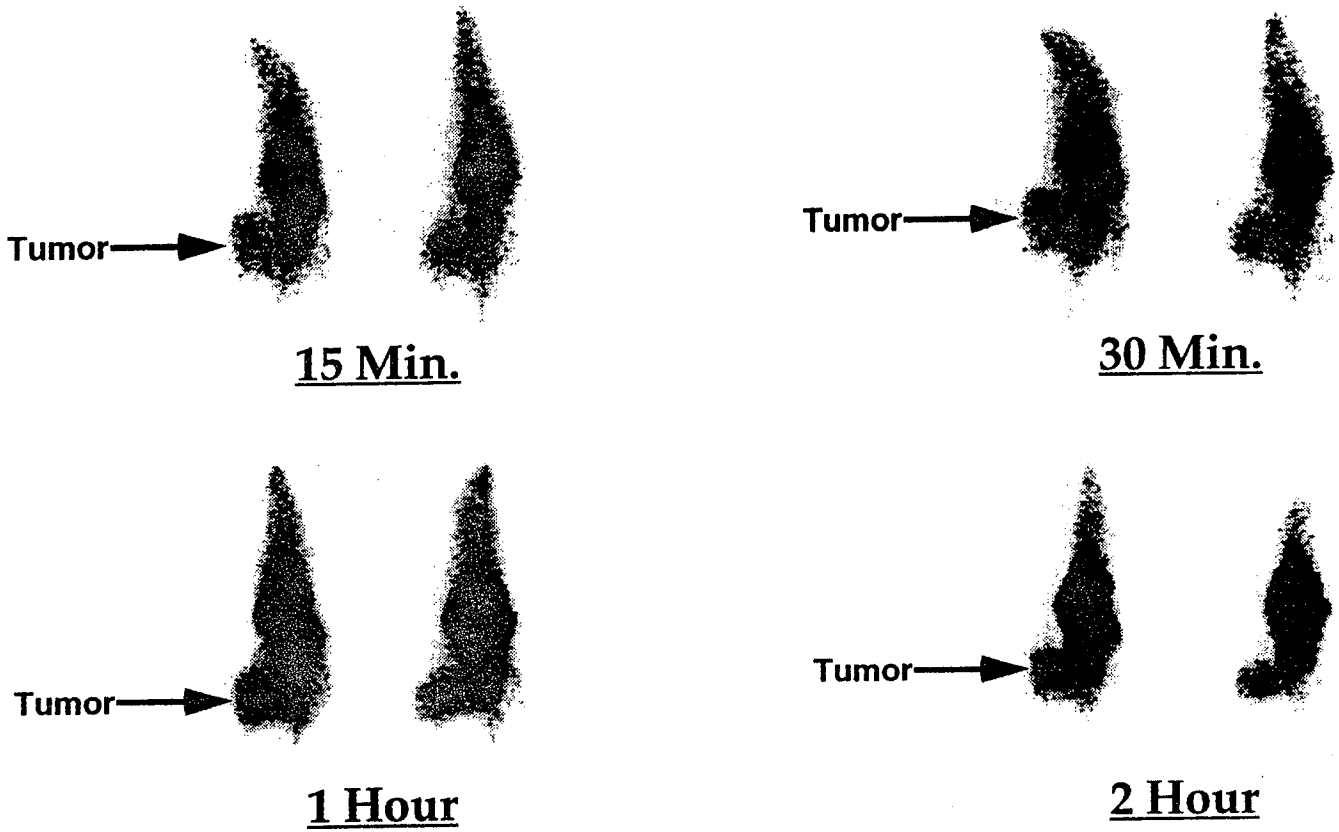


Figure 15C. Planar images of sarcoma-bearing mice (low apoptosis) after administration of $^{99m}$Tc-EC-NIM (100μCi/mouse, iv.) showed that the tumor could be well visualized from 15 minutes to 2 hours postinjection.

$^{99m}$Tc-EC-Nitroimidazole (NIM)
(100μCi/mouse, iv.)

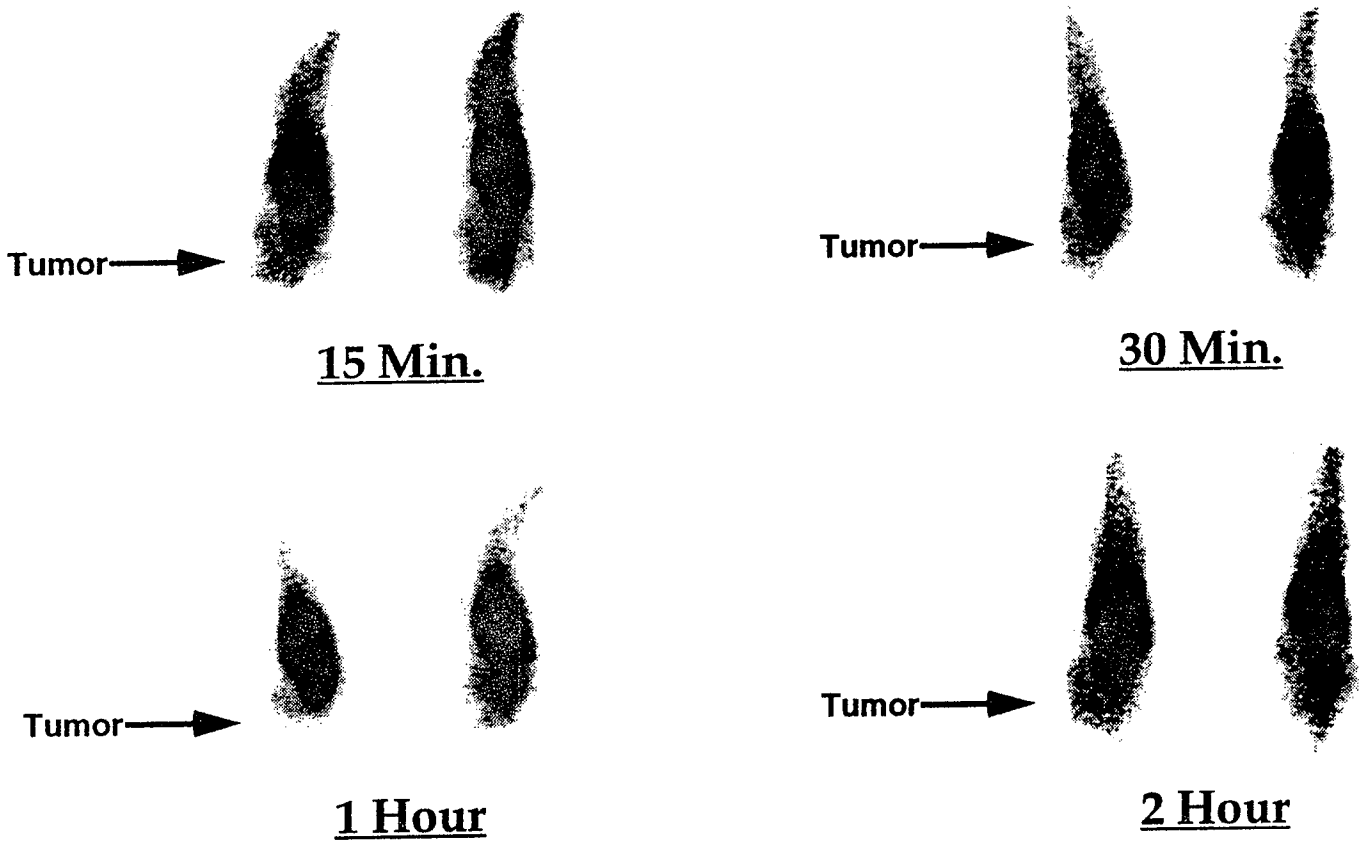


Figure 15D. On day 18, planar images of sarcoma-bearing mice (low apoptosis) after paclitaxel treatment (80mg/kg, iv., single injection on day 14) were taken.

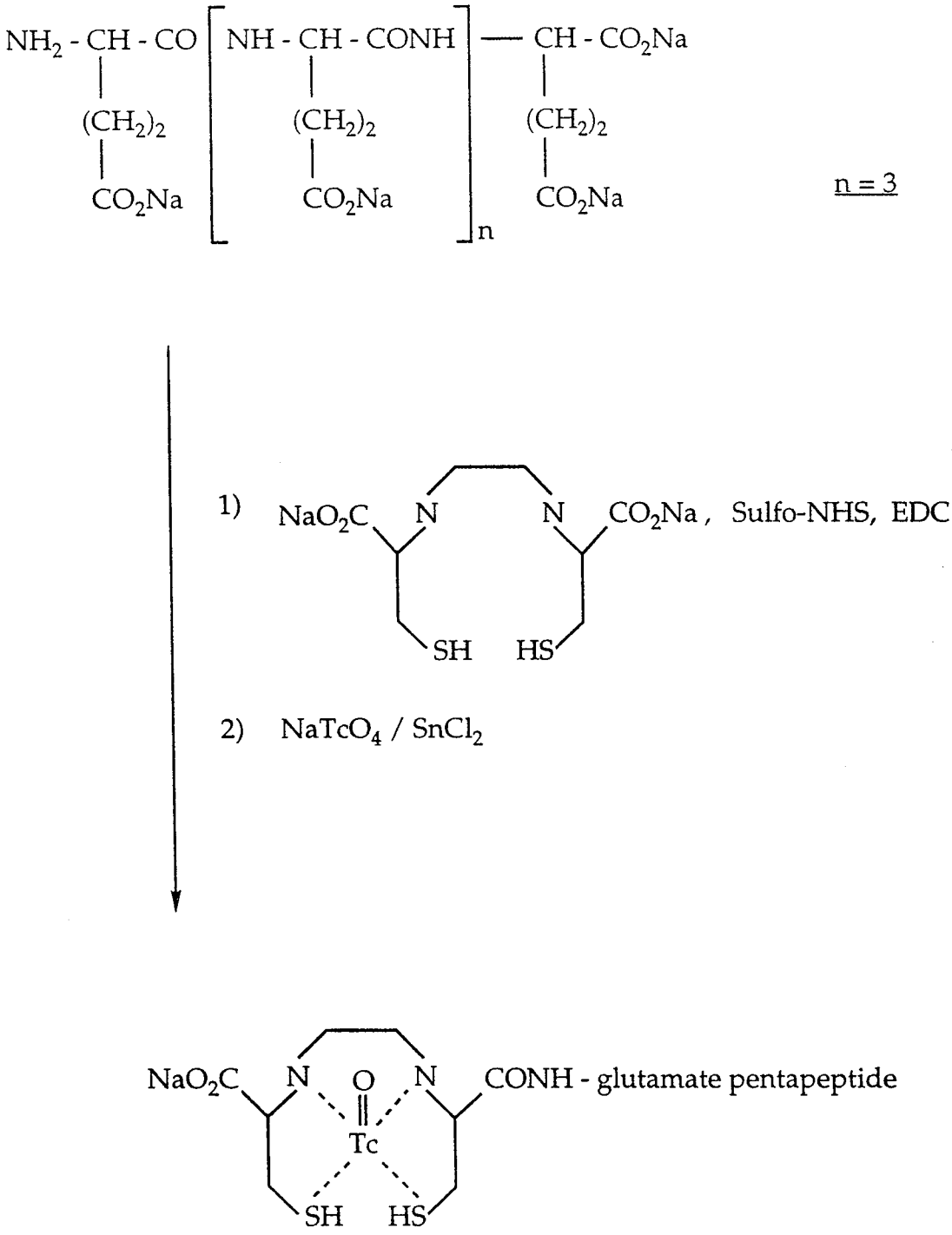


**Figure 16. Radiosynthesis of $^{99m}$Tc-EC-Pentaglutamate**

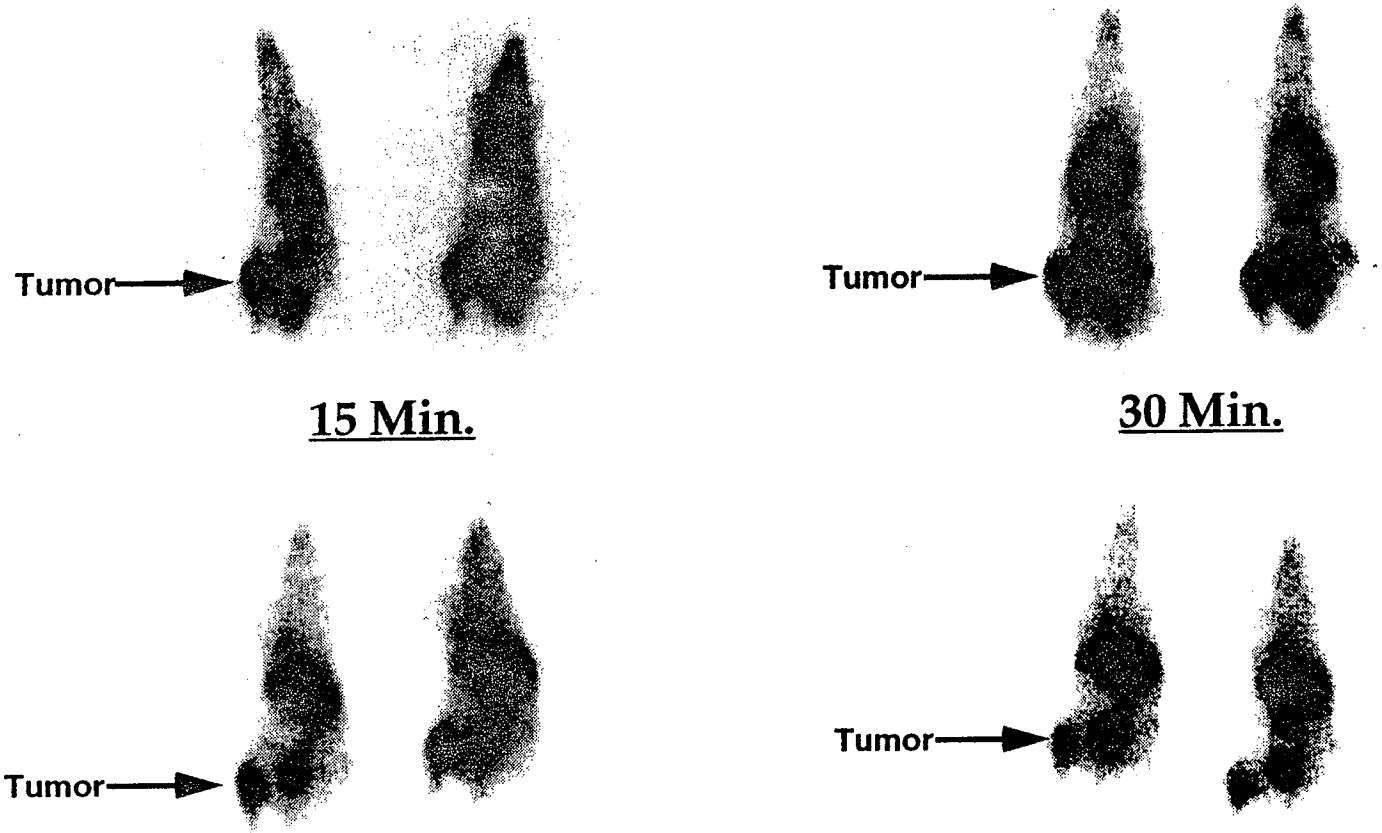


**Figure 17. Planar images of breast tumor-bearing rats following intravenous administration of $^{99m}$Tc-EC-Pentaglutamate (300μCi/rat) showed that tumors could be visualized from 15 minutes to 2 hours postinjection.**

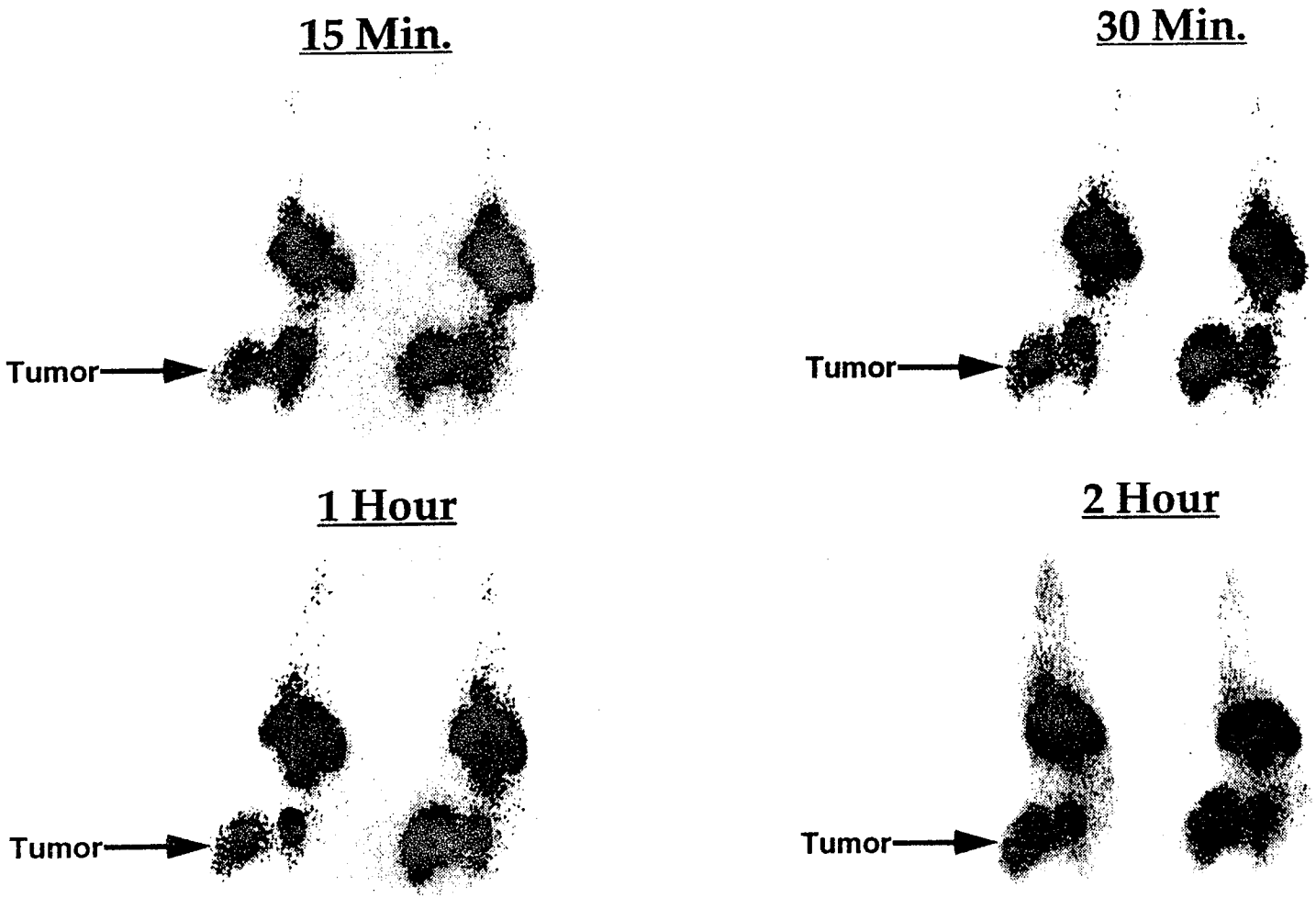


Figure 18. Planar images of breast tumor-bearing rats following administration of $^{99m}$Tc-EC-Annexin V (300μCi/rat, iv.) showed that tumor uptake could be visualized from 15 minutes to 2 hours.

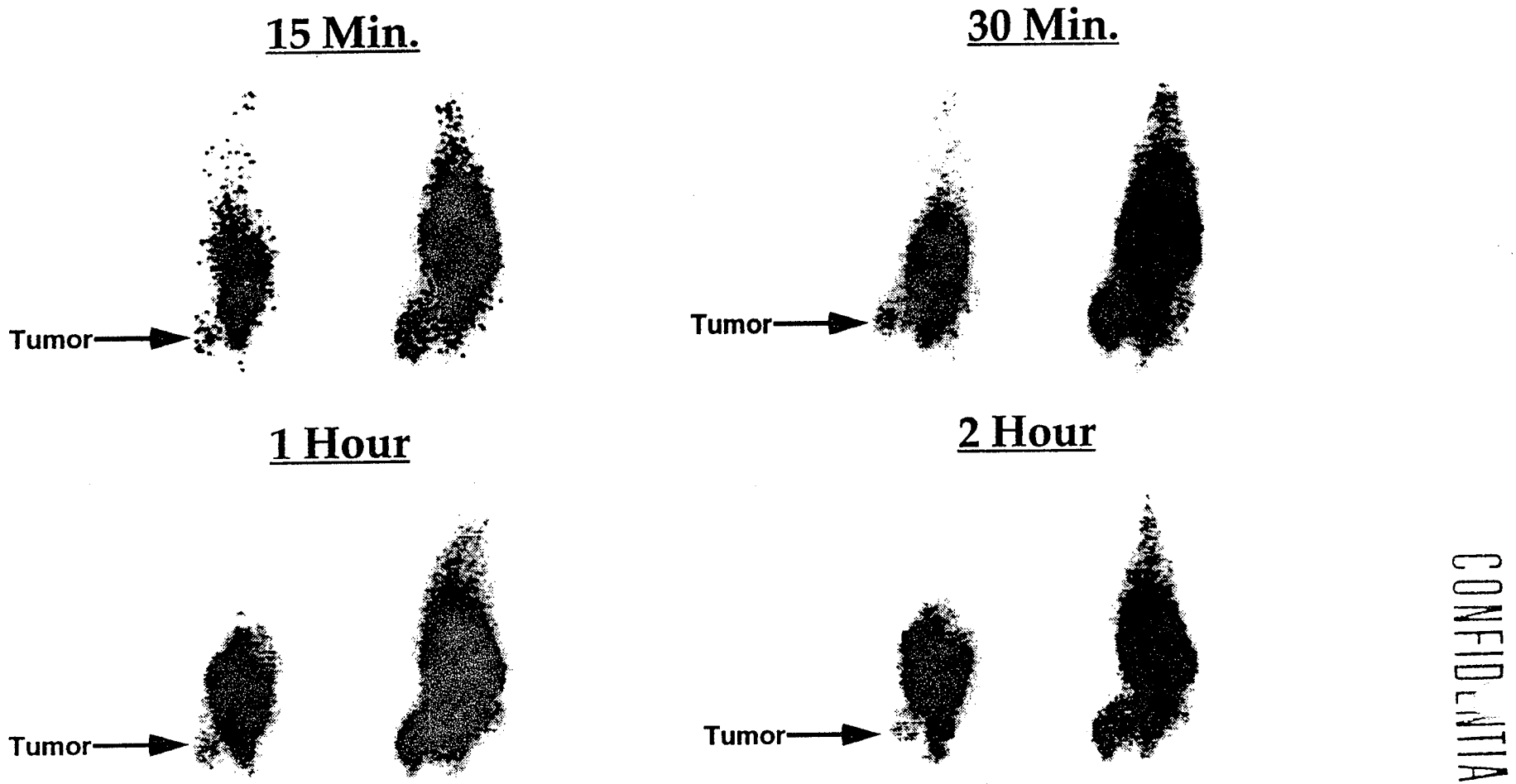




Figure 19A. Planar images of ovarian (OCA-1) tumor-bearing mice after administration of $^{99m}$Tc-EC (left) and $^{99m}$Tc-EC-Annexin V (right)(100μCi/mouse, iv.) demonstrated that the tumor could be visualized 15 min. postinjection with $^{99m}$Tc-EC-Annexin V.

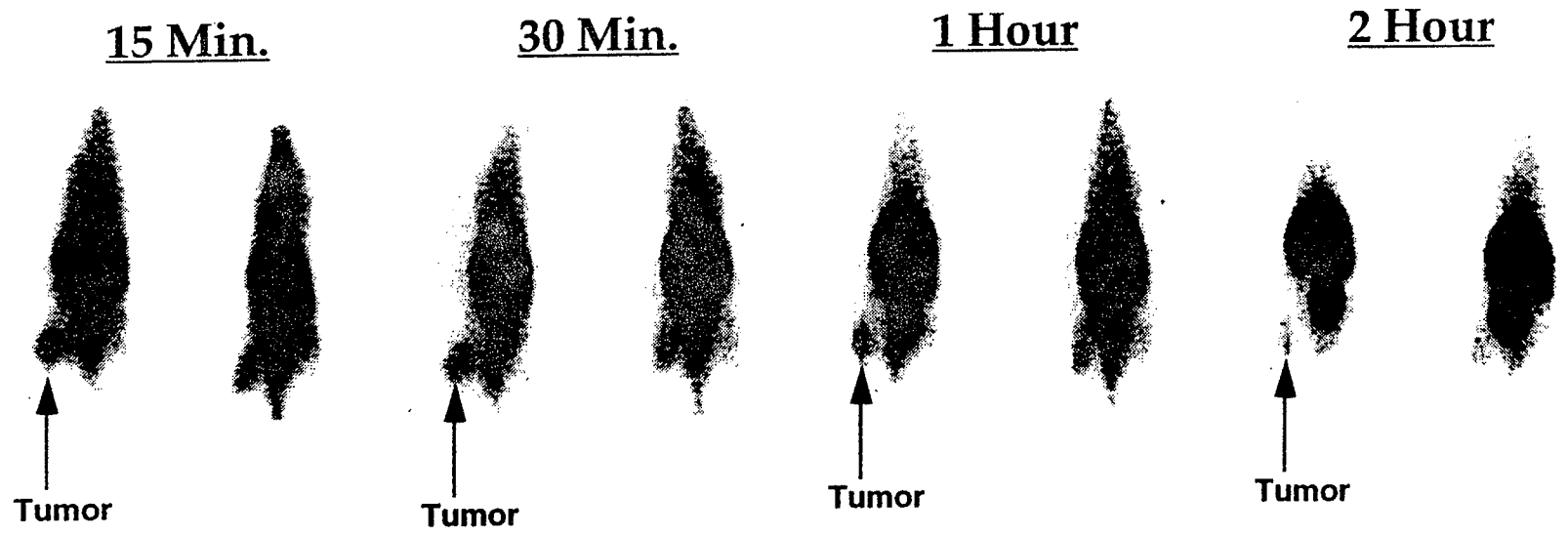


Figure 19B. On day 18, planar images of OCA-1 tumor-bearing mice (high apoptosis) after paclitaxel treatment (80mg/kg, iv., single injection on day 14) showed that the tumors had less uptake compared with the pretreatment data.

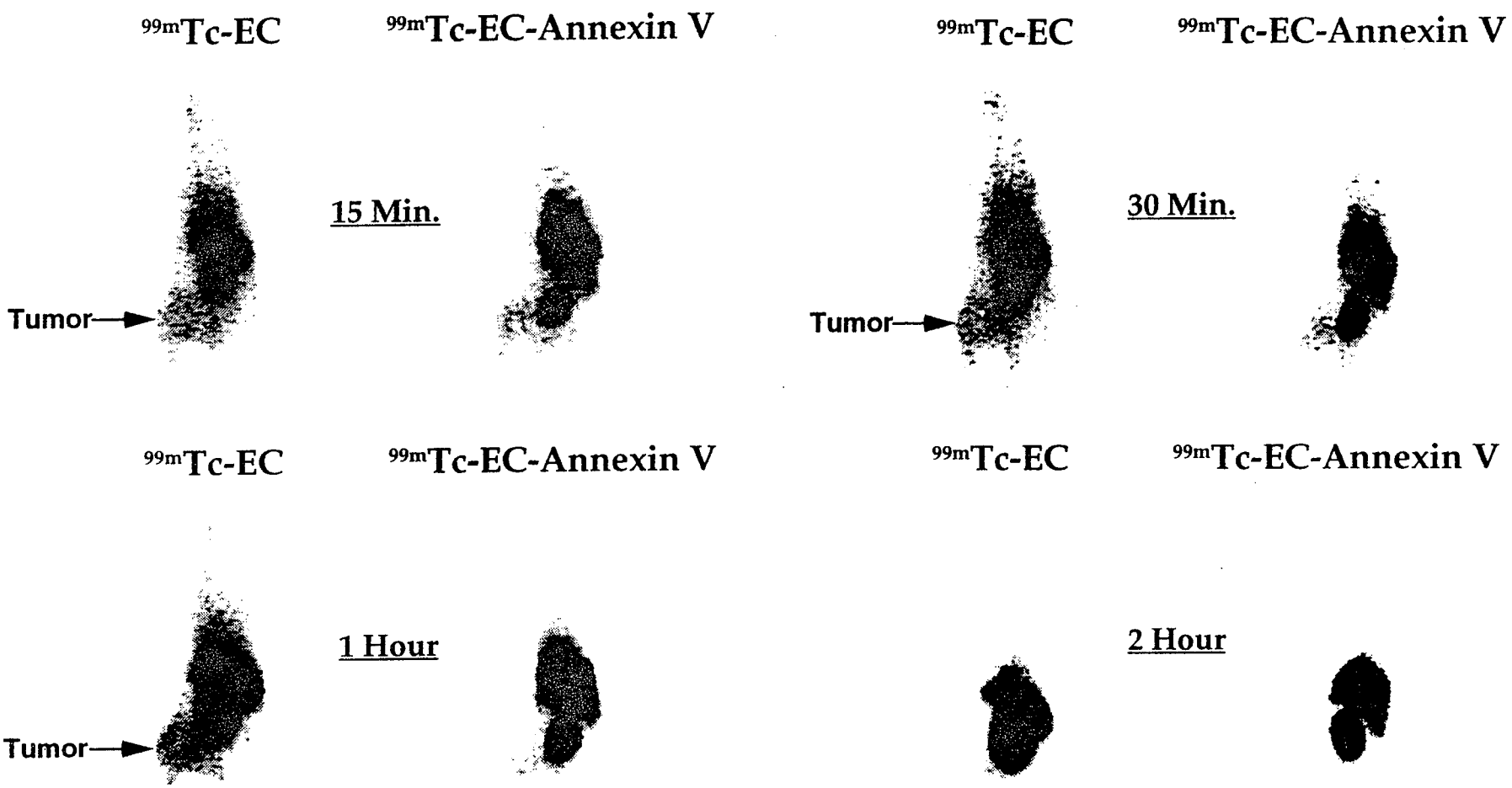




**Figure 20A.** Planar images of sarcoma-bearing mice (low apoptosis) after administration of $^{99m}$Tc-EC and $^{99m}$Tc-EC-Annexin V (100μCi/mouse, iv.) indicated that tumor uptake was low with both tracers.

# $^{99m}$Tc-EC-Annexin V
## (100μCi/mouse, iv.)

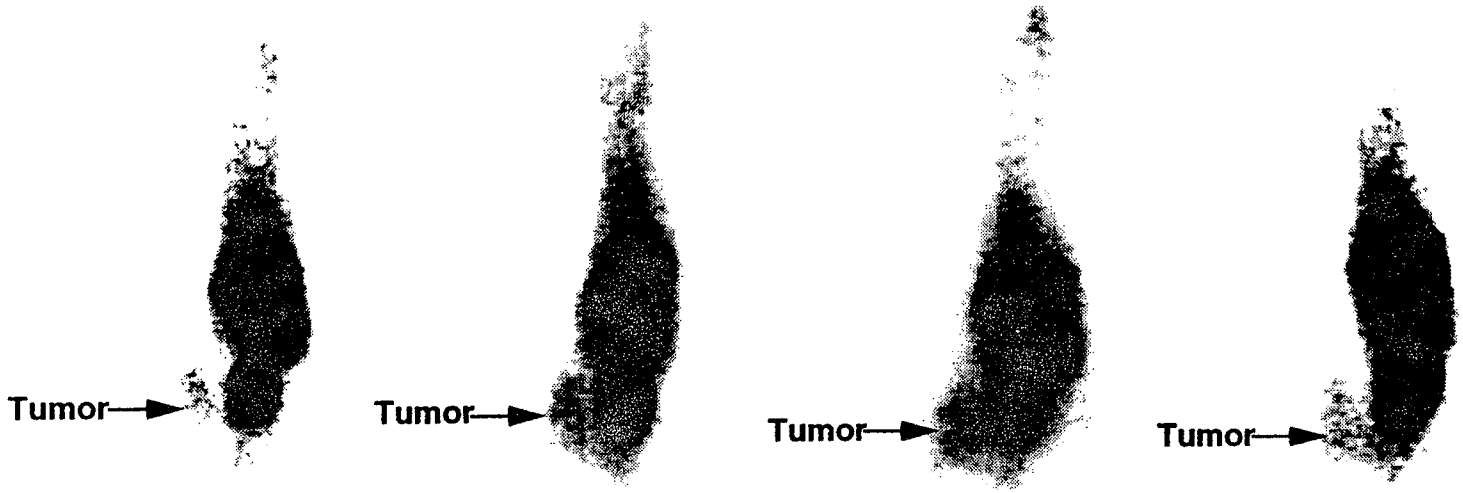


**15 Min.** **30 Min.** **1 Hour** **2 Hour**

Figure 20B. On day 18, planar images of sarcoma-bearing mouse (low apoptosis) after paclitaxel treatment (80mg/kg, iv., single injection on day 14) showed that the tumor uptake was low.

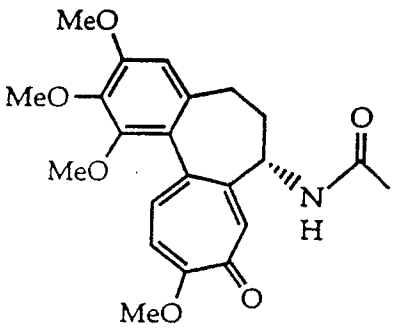

Colchicine (COL)

1) $H_2SO_4$ / $H_2O$

2) $Na_2CO_3$

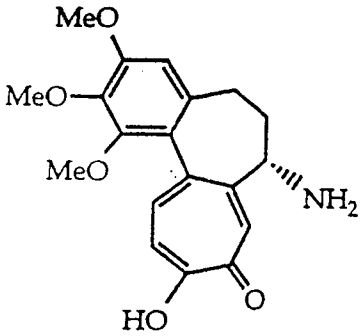

$COL\text{-}NH_2$

1) $COL\text{-}NH_2$

2)

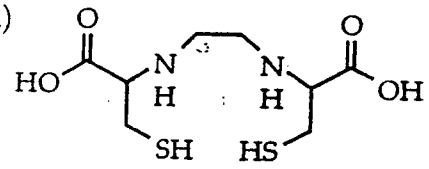

EC

3) 1N-NaOH

4) EDC-HCl / Sulfo-NHS

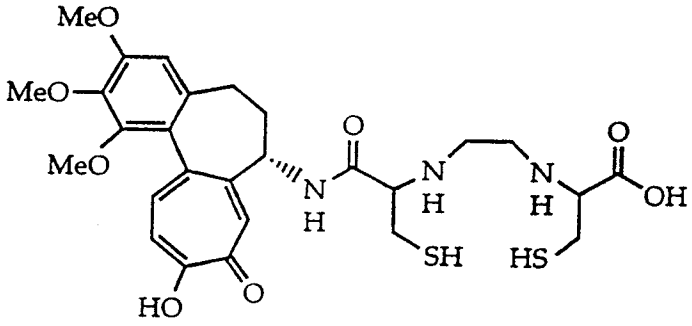

EC-COL

$Na^{99m}TcO_4$ / $SnCl_2$

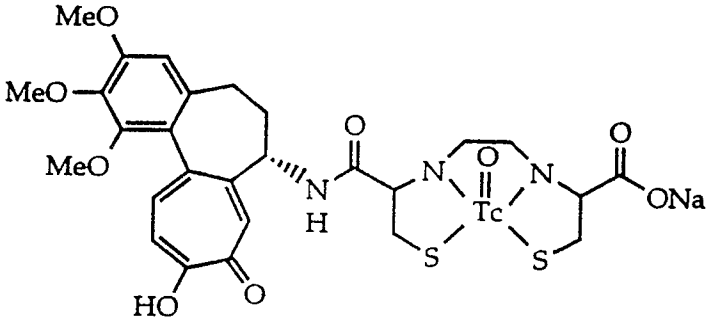

$^{99m}$Tc-EC-COL

**Figure 21.** Synthetic scheme of $^{99m}$Tc-EC-Colchicine.

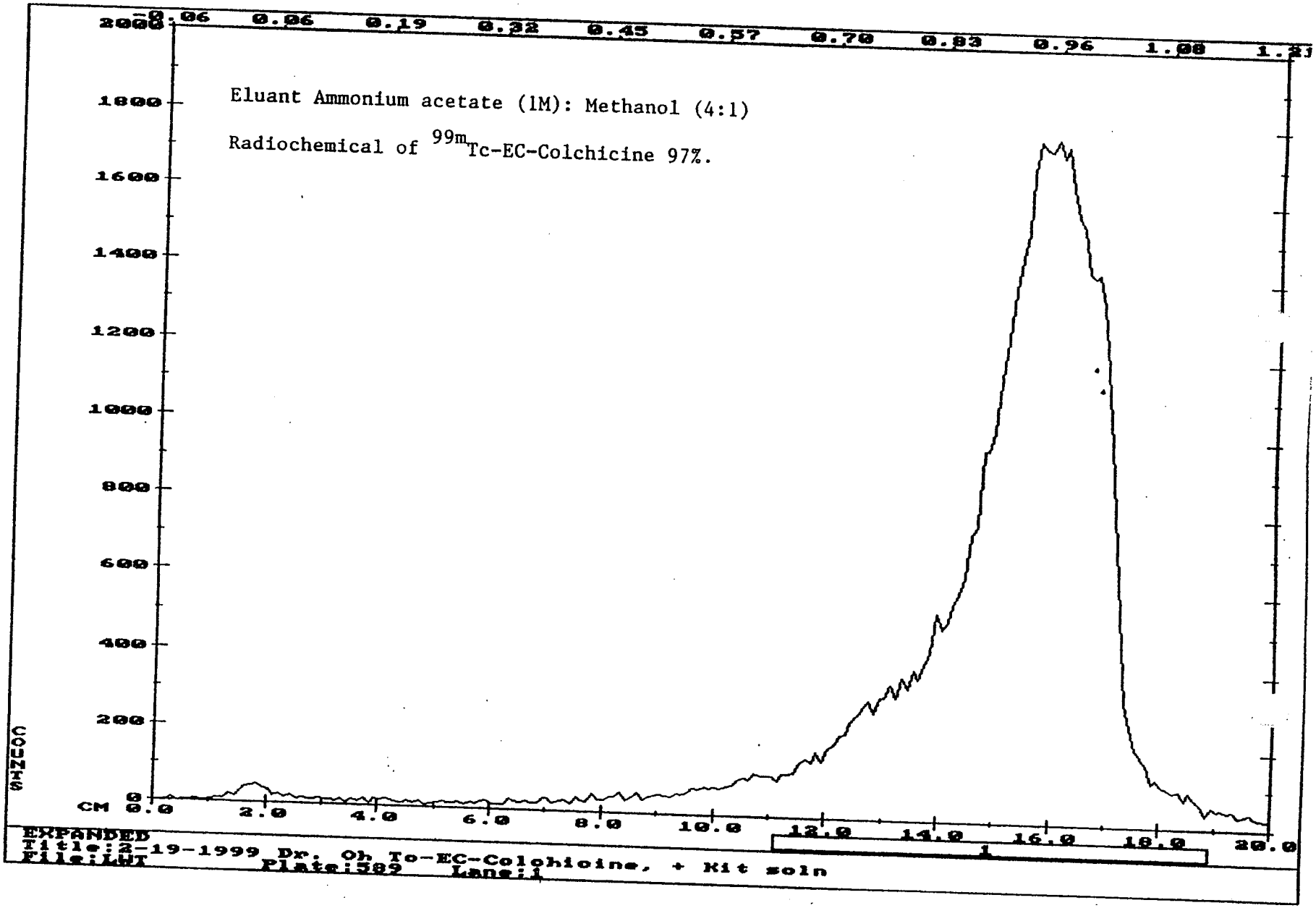


**Figure 22.** Radio thin-layer chromatography of $^{99m}$Tc-EC-Colchicine.

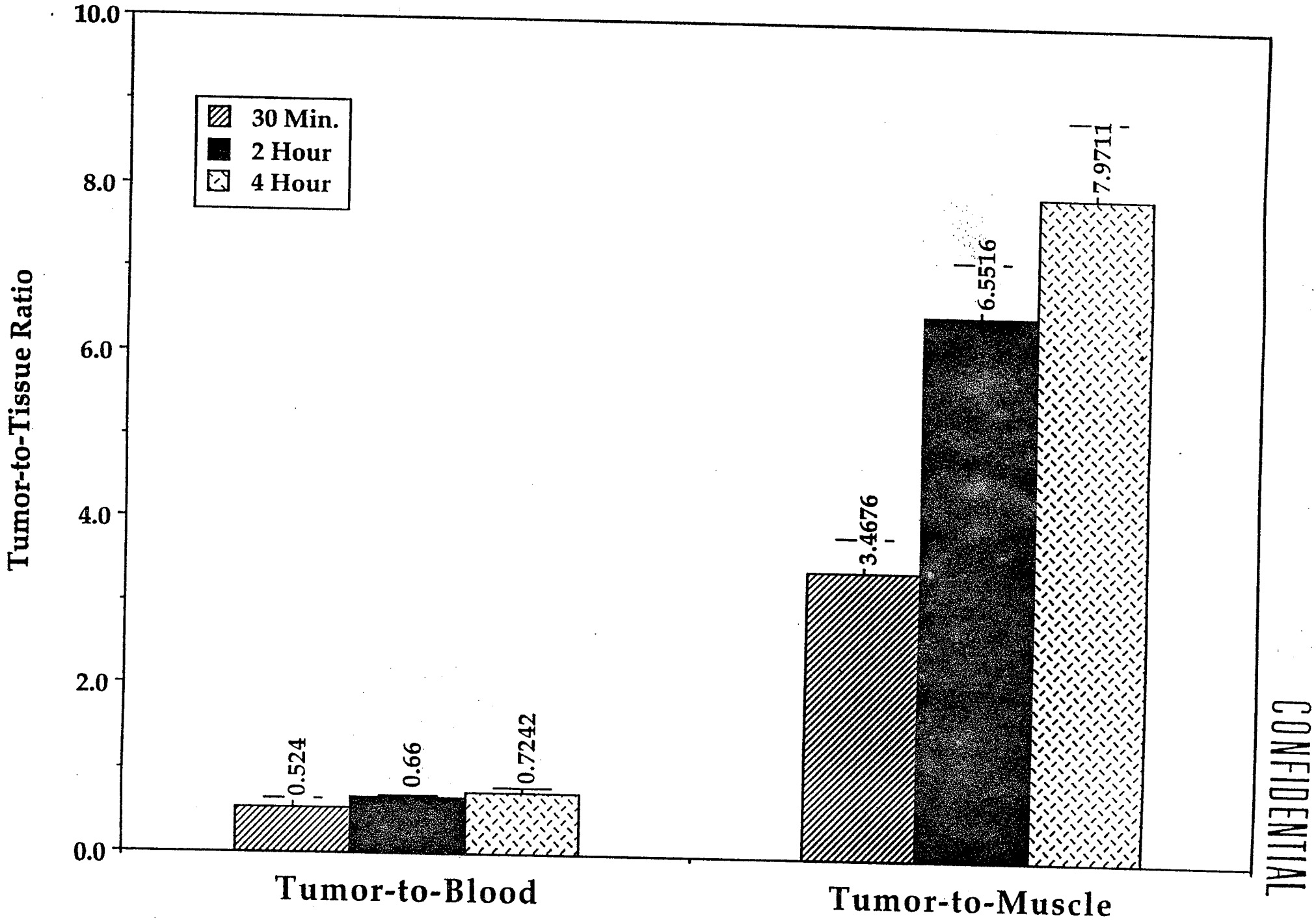


**Figure 23.** Tumor-to-blood and tumor-to-muscle count density ratios of $^{99m}$Tc-EC-Colchicine in breast-tumor-bearing rats as a function of time. Data are expressed as the mean± S.E. for

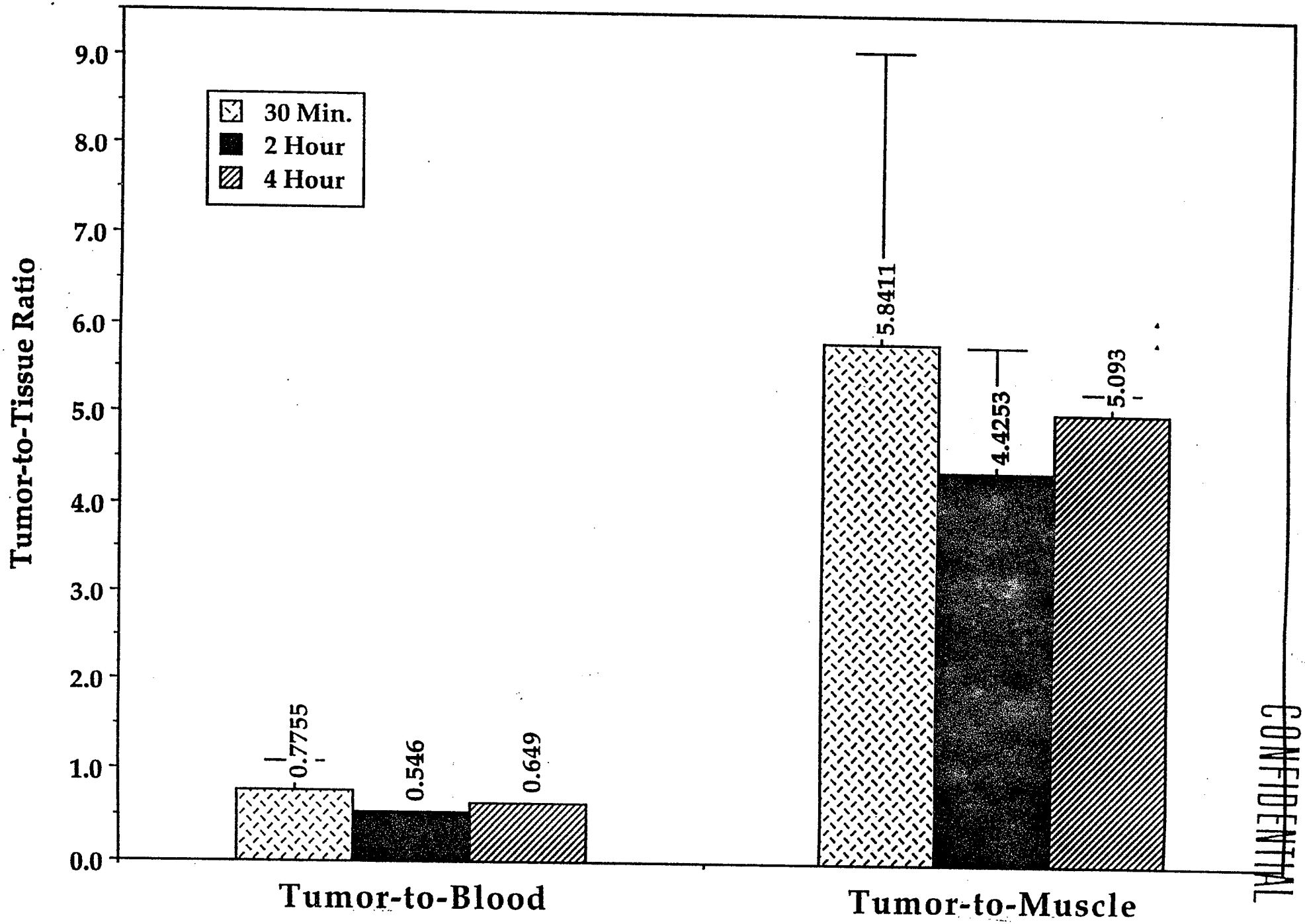


**Figure 24.** Tumor-to-blood and tumor-to-muscle count density ratios of $^{99m}$Tc-EC in breast-tumor-bearing rats as a function of time. Data are expressed as the mean+ S.E. for n=3 rats per

$^{99m}$Tc-EC-Colchicine (1 Hour Postinjection)

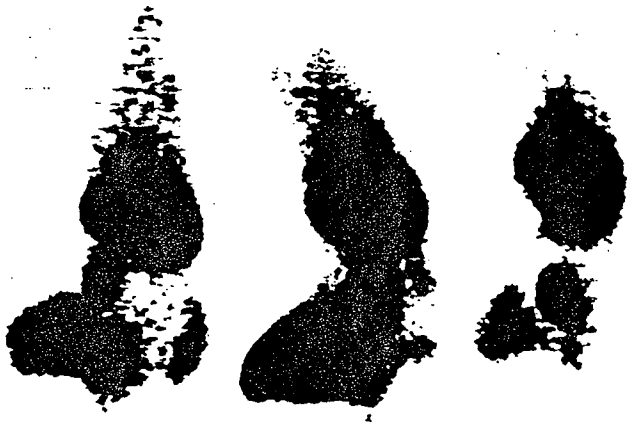

**Figure 25.** Anterior view of breast-tumor-bearing rats receiving $^{99m}$Tc-EC-Colchicine (300 μCi, iv.) showed that there was tumor uptake at 1 hour post-injection.

$^{99m}$Tc-EC (Control) (1 Hour Postinjection)

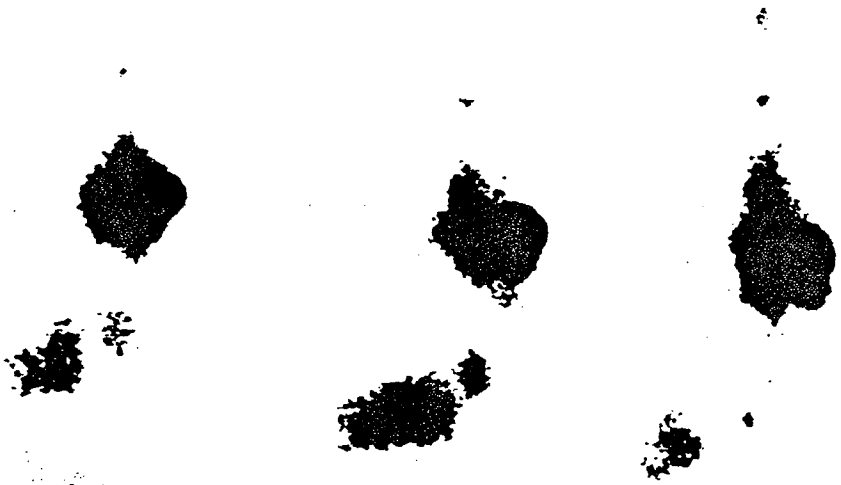

**Figure 26.** Anterior view of breast-tumor-bearing rats receiving $^{99m}$Tc-EC (300 μCi, iv.) showed that there was less tumor uptake at 1 hour post-injection compared to $^{99m}$Tc-EC-Colchicine.

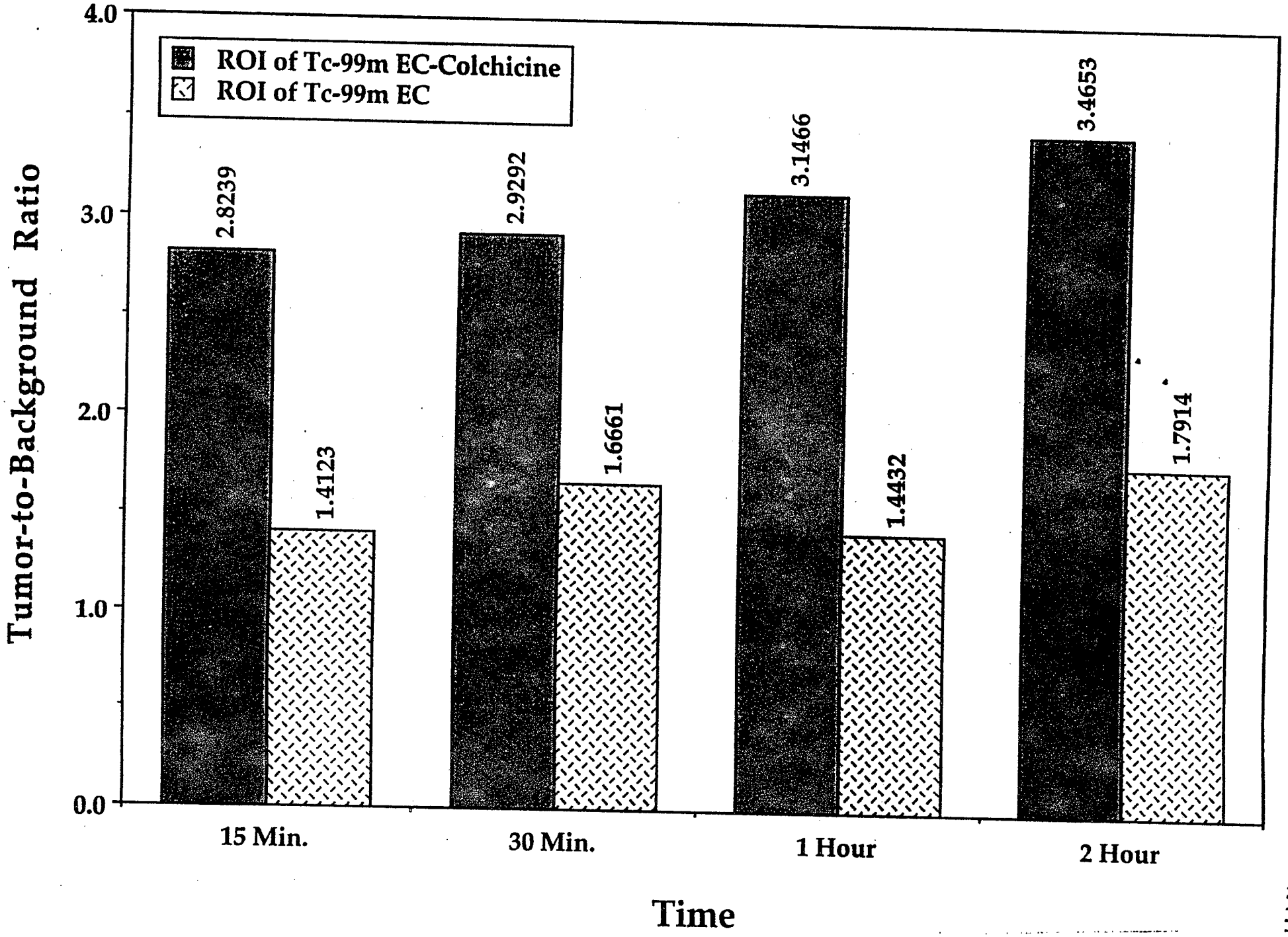


CONFIDENTIAL

**Figure 27.** Computer outlined region of interest comparison of tumor-tobackground ratios between $^{99m}$Tc-EC-Colchicine and $^{99m}$Tc-EC in breast-tumor-bearing rats.